A Review on Amorphous Noble-Metal-Based Electrocatalysts for Fuel Cells: Synthesis, Characterization, Performance, and Future Perspective.

Quoc Tuan Phan *[a], Kee Chun Poon [a] and Hirotaka Sato *[a]

[a] School of Mechanical & Aerospace Engineering, Nanyang Technological University, 50 Nanyang Avenue, Singapore 639798, Singapore.

E-mail: hirosato@ntu.edu.sg/phan0054@e.ntu.edu.sg

*Corresponding author

ABSTRACT

An urgent need for cleaner energy alternatives has driven the research of fuel cells, and consequently, electrocatalysts. Noble metals such as Pt and Pd are well known as the most suitable catalysts for fuel cell reactions. However, because of their high costs, much effort has been invested to improve their efficiency. Amorphous noble metal nanoparticles are promising electrocatalysts because of their abundant uncoordinated active sites that result from their long-range disordered lattice. Researches on amorphous Pt- and Pd-based catalysts have progressed well with several different synthesis routes. This review aims to systematically study the differences, advantages, and disadvantages of these methods and the resulting characteristics, performance in fuel cell applications, and future prospects of the amorphous Pt- and Pd-based catalysts.

Keywords:

Amorphous; Platinum; Palladium; Electrocatalyst; Fuel cells

Table of Contents

1. Introduction

Due to the ever-increasing energy demand and rapidly worsening situation of climate change, there is a dire need for alternative sources of energy that are clean and renewable [1]. Among other renewable energy sources such as photovoltaic cells and wind turbines, fuel cells have emerged as a promising contender and have long become a popular research topic for green energy [1, 2].

Having many advantages, fuel cells still have various issues that require improvements. The major challenge is that majority of the reactions involved (except for hydrogen oxidation reaction) at both electrodes are kinetically slow, although they are thermodynamically favored. This is due to high activation energy barriers of the rate-determining steps, namely, cleavage of strong stable bonds such as C–H and O=O [1, 3, 4]. Therefore, catalysts are essentially always required to increase the rates of these sluggish reactions.

Noble metals such as Pt and Pd are considered the most widely used electrocatalysts for both oxidation and reduction reactions [1, 3]. Even though much effort has been spent on exploring low-cost catalyst materials for ORR, however they suffer from poor stability, conductivity and complex syntheses [5-25]. Being the most popular electrocatalysts for fuel cells with high catalytic activity, Pt and Pd still have several shortcomings that hinder their potential as catalysts for fuel cells. First, they are extremely rare and thus expensive metal, so their mass activity, which is catalytic current peak normalized by weight of catalyst, should be optimized [1, 3, 26]. In addition, they have poor durability due to poisoning by reaction intermediates, especially in the case of alcohol or formic acid oxidation [3, 26]. It has been hypothesized that carbon monoxide (CO) formed during the intermediate stages of the oxidation reaction can bind itself strongly to the catalyst's active sites and deactivate them [27]. Oxidative removal of CO is difficult as it requires large overpotential, slowing down the reaction even further [28]. Therefore, strategies need to be developed to overcome these challenges.

There have been several reported approaches that tackled these issues. Popular directions focus on controlling the catalysts' shapes [29-34] and morphologies [35-38] and developing multimetallic alloys [39-42] or even special support materials [43-47]. By manipulating the catalysts' shapes, researchers have shown that by increasing the exposure of high-index facets, catalytic activity can be increased [30, 33, 48-51]. In addition, hollow 3-D shapes of catalysts can vastly improve their mass activity due to the exposure of their inner surface [29, 31, 34, 52-57]. Porous morphology can also increase catalytic activity by increasing the available catalytic surface area and promote mass diffusion [35-38, 58-62]. Furthermore, researchers have intensively explored alloying Pt and Pd with transition metals such as Ru, Ni, and Cu [29, 30, 32, 34, 41, 53, 63-66]. Transition metals are inexpensive, thus can reduce cost of the catalysts. They increase catalytic activity of the catalysts via two mechanisms: (1) their oxophilicity and (2) weakening of the bond between poisonous CO intermediates and catalyst due to decreased electron density of Pt and Pd [39, 51, 53, 63, 67-71]. Lastly, although support materials do not directly participate in the catalytic process, they can improve overall reaction kinetics because they facilitate mass diffusion. In addition, some functionalized support materials can influence the final composition of the catalysts during synthesis. For example, carbon nanotubes (CNTs) treated with concentrated HNO_3 (O-functionalized CNTs) can increase the amount of P-doping in Pd-P nanoparticles (NPs) [72]. Novel support materials can be generally divided into two groups: those that are novel carbon based such as reduced graphene oxide, N-doped graphene, and functionalized graphene [42, 47, 73, 74] and those that are noncarbon supports such as titanium nitride nanotubes, Mo-doped titanium nitride, and titania [43-45].

One of the most recent approaches in the design of effective catalysts is the development of Pt- and Pd-based amorphous catalysts. Amorphous structure is unique with many interesting properties. It is characterized by many defects due to long-range disordered lattice. These defects have low-coordination active sites, which have been reported to increase catalytic activity [75, 76]. In addition, the synergistic effects of doping and alloying elements that are added to the lattice to create

amorphous structure also contribute to higher catalytic activity. Therefore, amorphous catalysts have improved activity compared to their crystalline counterparts.

In this report, different synthesis methods, characterization, performance, and future prospects of amorphous noble-metal-based catalysts are reviewed in order to shed light on how amorphous catalysts are formed and how their properties contribute to their superior performance in fuel cell applications.

2. Synthesis methods (description, explanation, and insights)

Amorphous, or metallic glass, structure is characterized as having a lack of any long-range ordered lattice that is normally observed in crystals. Therefore, the first principle that all synthesis methods for amorphous structure must follow is that the lattice must be distorted, whether by physical or chemical means. Amorphous phase is however a metastable state, unlike the stable crystalline phase. This means that all amorphous materials synthesis methods must be able to follow second principle, which is to prevent crystal formation. In this section, different strategies used to achieve the goals set out by these two principles are discussed in terms of their formation mechanisms as well as their advantages and disadvantages.

2.1. Top–down approaches

2.1.1. Conventional methods

Conventional top–down methods for the synthesis of amorphous materials follow the concept of "energize and quench" in order to process the materials at a non-equilibrium state (amorphous phase is non-equilibrium metastable phase). Basically, the materials are supplied with energy to bring them from an equilibrium crystalline state to a highly non-equilibrium state and then quenched to the desired metastable phase [77]. Amorphous catalysts synthesized using these conventional methods belong to the category of bulk amorphous metal alloys, or bulk metallic glass.

Mechanical alloying is a powder-processing technique that utilizes repeated cold welding, fracturing, and rewelding of powder particles in a high-energy ball mill. This technique enables the synthesis of a variety of equilibrium and non-equilibrium alloy phases including amorphous alloys [77-80]. Although the concept is simple, this process is extremely time consuming (normally takes 40 h of milling) and extremely energy intensive. Moreover, it is wasteful. In order to prepare the catalyzed electrodes, the amorphous alloy powders are mixed with glassy carbon and paraffin binder. This means that a large amount of the catalysts is left inside the bulk of the electrode and is not being fully utilized [81].

Melt quenching is a traditional method used to produce amorphous metal alloys. The idea behind this method is simple: a mixture of molten metals is cooled down at a rate fast enough to prevent crystal formation, and the materials are locked in a metastable glassy state. The cooling down rate is normally in the range of millions of degrees per second [82-84]. This method, although faster than mechanical alloying, is still energy intensive.

2.1.2. Dealloying method

Dealloying is a top–down process used for the fabrication of amorphous catalysts with nanoscale features, which are known as nanoporous catalysts. Catalysts synthesized via this method are commonly Pd based, belonging to category of dealloyed amorphous Pd-based metal alloys.

Essentially, this method does not induce amorphous structure. Its main purpose is to increase the surface area of the catalyst while maintaining its amorphousness. In general, an amorphous alloy is formed with an extra metal in ribbons. These ribbons are then soaked in concentrated acid (e.g.,

sulfuric acid) to dissolve, or dealloy, the extra metal, leaving the wanted metals behind. These metals undergo sulfurization in a two-step mechanism. Depending on what element the extra metal is, dealloying process can be carried out in two steps: first in strong base and then in concentrated acid [85, 86].

Another variation that allows better control of the removal of the extra metal is selective etching by anodic polarization in diluted acid (e.g., 0.5 M H_2SO_4). By adjusting the potential, etching of the noble metal can be greatly eliminated, hence reducing the number of control parameters (e.g., dissolution of noble metals) [87].

Although low processing temperature plays a role in maintaining crystallinity, it is believed that the difference in diffusion coefficients of metals (in this case, Pd has a lower diffusion coefficient than Cu) results in a "fixing" effect, keeping all the atoms in place and preventing them from crystallizing. It was proven in a previous study that when only one metal is used (Cu), the structure recrystallizes [85, 86].

The ratio of the metals used in the precursor has an effect on amorphousness. For amorphous Pd-Cu-S, the starting precursor $Ti_{30}Cu_{68}Pd_2$ is required, while $Al_{80}(Pd_{0.67}Cu_{0.33})_{20}$ could not yield amorphousness. The starting precursor $Al_{80}Pd_{10}Cu_5Ni_5$ with a lower Pd concentration, interestingly yields an amorphous structure. This phenomenon has two advantages: (1) amorphous structure with a high catalytic activity is achieved and (2) cost savings is gained because lower Pd concentration is used.

2.1.3. Thermal plastic forming (TPF) techniques

TPF is an innovative top-down method to synthesize metallic glass (or amorphous) nanostructures from bulk metallic glass. It is a net-shaping fabrication method, along with direct casting. Compared to TPF, direct casting of molten metals into molds followed by rapid cooling yields poor fidelity and limited shapes, thus is not well investigated and will not be discussed in great details here [88-90].

TPF is carried out by heating bulk metallic glasses to a specific supercooled liquid state, then shape it using a variety of techniques conventionally used for thermoplastic forming, such as molding, extrusion, blow molding, rolling, etc. with molding or imprinting being most extensively reported thanks to the complex shapes that this technique can achieve. For imprinting, the supercooled liquid state metallic glass fills in templates to get desired shapes and dimensions [88, 89, 91-94]. Bulk metallic glasses can exist in a supercooled liquid state at a temperature above their glass transition temperature without crystallization. This state of viscous liquid is stable across a large temperature-time range, which allows an opportunity to shape them using. Discovery of bulk metallic glass alloys with high formability and utilization of wetting between the mold and the metallic glass has led to fabrication of nano-dimension structures [88, 91, 94]. Such techniques are often referred to as nanoimprinting or nanomoulding in literature.

The most profound strength of these techniques, especially nanoimprinting/nanomoulding, is their high-throughput for complex, even hierarchical nano-sized structures. Nonetheless, they are not without limitations. There are limited options for materials because not all elements used in alloys can form metallic glass, and not all metallic glasses have the suitable formability for processing [94]. Efforts have been spent on investigating post-processing techniques such as galvanic displacement, electrochemical deposition and underpotential deposition to incorporate elements that are unable to form glass [94, 95].

2.2. Bottom–up approaches

The main disadvantage of using noble metals such as Pd and Pt as catalysts is their limited availability and thus exorbitant price. This has been one of the main reasons why fuel cells are not fully commercialized.

The solution to reduce the use of these noble metals is to maximize their surface area, since their catalytic properties are strictly surface processes. For spherical particles (the typical nanoparticle shape), their surface area is inversely proportional to their radius. Therefore, to maximize the surface area of the catalysts, the size of these catalysts needs to be reduced to increase the area/volume ratio.

Achieving a smaller particle size is the biggest challenge for top–down approaches. Although they are easily implemented in industrial settings, there is a limit on the catalyst particle size that can be obtained. Whether it is due to theoretical limit, lack of advanced equipment, or cost of production being too high compared to the cost saved from reducing noble metal use, there exists a bottleneck for top–down approaches. Therefore, bottom–up approaches are a more suitable option.

2.2.1. Wet chemical reduction

Wet chemical reduction is a simple method to synthesize amorphous catalysts. Generally, the synthesis requires two main components: metal precursors and reducing agents. Metal precursors include ionic forms of Pd, Pt, and transition metals for alloying. Reducing agents are used to reduce the metal ions to their metallic state. Other secondary components such as surfactants and pH regulators can also be incorporated to fine-tune the characteristics of the catalysts. The reagents can be mixed in different combinations and ratios to achieve the desired composition of the final catalysts. To achieve amorphous structure, the composition of each component has to fall within a certain critical range. Phosphorus doping plays a critical role in achieving amorphousness by inducing lattice disorder. The discovery of doping phenomenon is due to the use sodium hypophosphite (NaH_2PO_2). It was found out that NaH_2PO_2 can undergo reduction to elemental P alongside with metal ion reduction [96, 97]. Catalysts synthesized via this method therefore belong to the category of P-doped nanocatalysts. Alloying transition metals also create a lattice mismatch that aids in the induction of amorphous structure.

Efforts to fabricate amorphous metal alloys dated back in 1997 [98], where catalysts were fabricated in the form of a 5-µm coating instead of smaller nanoparticles. Fortunately, the size of the catalysts obtained from bottom–up approaches can be controlled simply via time, which is a great advantage, as evident with the results of a study by Salomé et al. [6]. These authors reported the synthesis of a PdP catalyst deposited on a carbon paper for a significantly reduced deposition time. These catalysts had an agglomerate size of 100–200 nm.

Due to the simplicity of bottom–up approaches, they are widely used in the synthesis of not only amorphous but all types of catalysts. They also give researchers the flexibility to investigate different types of support materials. Besides the intrinsic properties of catalysts, it is well known that catalyst and support material interaction can increase catalytic activity as well [42-45, 47, 72-74].

Nevertheless, catalysts prepared by wet chemical reduction are still limited to small quantities used in research facilities. Fortunately, an interesting adaptation of bottom–up approaches developed by Poon et al. [75, 76], which is called stepwise electroless deposition, is fully automatable, showing a great promise for wide industrial applications. This process allows for the direct deposition of Pd-P on any substrate without pretreatment or preseeding and without the use of a chelating agent, which might hinder the catalytic activity of the catalyst.

2.2.2. Innovative methods

The catalysts that belong to this category are synthesized through different innovative methods. These catalysts are not yet well studied compared to the other three categories, but they hold a great promise of creating a breakthrough in the field of amorphous catalyst design and synthesis.

A recent approach to achieve amorphous Pd or Pt electrocatalyst is by using ligand exchange. The general procedure involves synthesizing a precursor, which is a crystalline catalyst, using wet reduction or solvothermal method. The shape of the formed precursor depends on the capping or ligand agent used. The ligand-exchange process is carried out by introducing a special ligand called bismuthiol I. This thiol ligand has a stronger interaction with Pd atoms, so it can displace other ligands bonded to Pd. It induces amorphousness at the outer layer of the catalysts. Then, the lattice gradually expands and transitions to an amorphous structure with time, without changing the morphology (shape) of the catalysts [99]. The ligand-exchange process has the advantage over the other methods already discussed because it can create shapes other than sphere or clusters normally obtained by other methods. So far, it has been reported that nanosheet and nanocubes can be obtained using this process [99].

Photolysis is the decomposition or separation of molecule driven by energy from light. A recent study has shown that amorphous Pt in thin film form can be synthesized using this method: a Pt complex (platinum β-diketonate) is synthesized, and spin coated onto a silicon or ITO substrate. Then, the complex is irradiated with UV light to decompose and yield an amorphous Pt film [100]. Although there is no explanation reported on the formation mechanism of the amorphous structure, it is a unique way to synthesize amorphous Pt. This method has a great advantage of practicality as spin-coating technique is well developed in the industry, so integration of this method for commercialization will be easier compared to other methods.

Galvanic displacement reaction is used as a technique typically for the synthesis of hollow and porous metal nanoparticles. The nature of this reaction is corrosion driven by the difference in electrochemical potentials between two metals. Typically, the synthesis involves a metal serving as a sacrificial template as well as a solution containing metal ions that are to be deposited. The metal ions will be reduced to metal, gradually displacing the metal that serves as a sacrificial template, which, on the other hand, will be oxidized to metal ions. Usually, galvanic displacement results in a crystalline structure. However, the special galvanic displacement of Cu by H_2PtCl_6 aided by $Na_2S_2O_3$ surprisingly yields amorphous CuPt alloy [101]. $Na_2S_2O_3$ is a complexing agent for CuCl. Therefore, the presence of $Na_2S_2O_3$ in the galvanic displacement of Cu encourages the formation of CuCl, where Cu has a valence state of +1 and prevents its disproportionation to Cu^{2+}. Therefore, for every four electrons needed to reduce $PtCl_6^{2-}$ to one Pt atom, four Cu atoms should be oxidized. The large discrepancy between the number of Cu atoms removed and the number of atoms of Pt formed creates a large number of lattice vacancies, increasing the surface energy of the system. As a result, the atoms rearrange into an amorphous structure that has lower energy than a heavily defected crystal structure.

Even though the mechanisms which form the amorphous structure are unique and innovative with many advantages, these methods suffer from limited materials options as they have only been discovered on a case-by-case basis and there is not yet a generalized strategy. Much work is needed in the future to explore their full potential as general synthesis strategies for amorphous structures.

3. Characterizations

The physical properties of catalysts are responsible for their catalytic performance, and the properties of interests are morphology, crystal structure, and chemical composition. Amorphous Pt- and Pd-based catalysts are subjected to the same characterizations. Aside from the absence of any long-range crystal structure (being amorphous) as the common property, other properties of amorphous Pt- and Pd-based catalysts discussed here are diverse because they are based on the results of different synthesis methods. This section aims to systematically discuss how amorphousness is characterized and to highlight some interesting differences among catalysts.

3.1. Amorphous structure

Amorphous structure is essentially indicated by the lack of any crystal structure. Therefore, to characterize amorphousness, techniques that are used to characterize crystal structure are used to look for proof for the lack of it. X-ray diffraction (XRD) is unarguably the most conventional and straightforward technique to study crystal structure. While it still holds an essential role in investigating nanocatalysts, XRD has its limitations. Because of the small size of nanoparticles, broadening of the diffraction peaks according to Scherrer's equation becomes significant, thus making interpretation of XRD spectra confusing. Therefore, additional proofs are often required, and in order to solve this problem, transmission electron microscopy (TEM) has been used to capture and evaluate the structures of catalysts.

Selected area electron diffraction (SAED) technique is commonly used to check for the amorphous structure of the nanoparticles. An amorphous structure is indicated by diffused rings, unlike the clear Debye–Scherrer rings that are characteristic of a crystalline structure. In Fig. 1, SAED images give information on the phase transformation of PtNiP particles annealed at different temperatures.

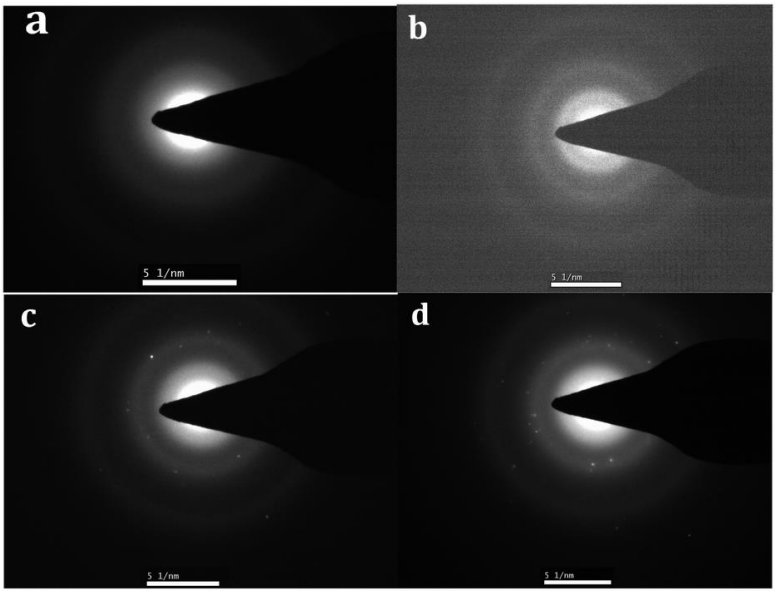

Figure **1** The SAED images of the amorphous $PtNiP_a$/C (a), and PtNiP catalysts annealed at different temperatures: PtNiP-300/C (b), PtNiP- 500/C (c) and PtNiP-700/C (d).Reprinted from reference [102] with permission from PCCP. Copyright (2014) of PCCP

More advanced techniques such as high-resolution transmission electron microscopy (HR-TEM) are also routinely used to double confirm the amorphous nature of nanoparticles. As shown in Fig. 2, an HR-TEM image of a catalyst reveals a fingerprint-like pattern that lacks clear lattice fringes of an orderly structure, indicating that the catalyst is indeed amorphous.

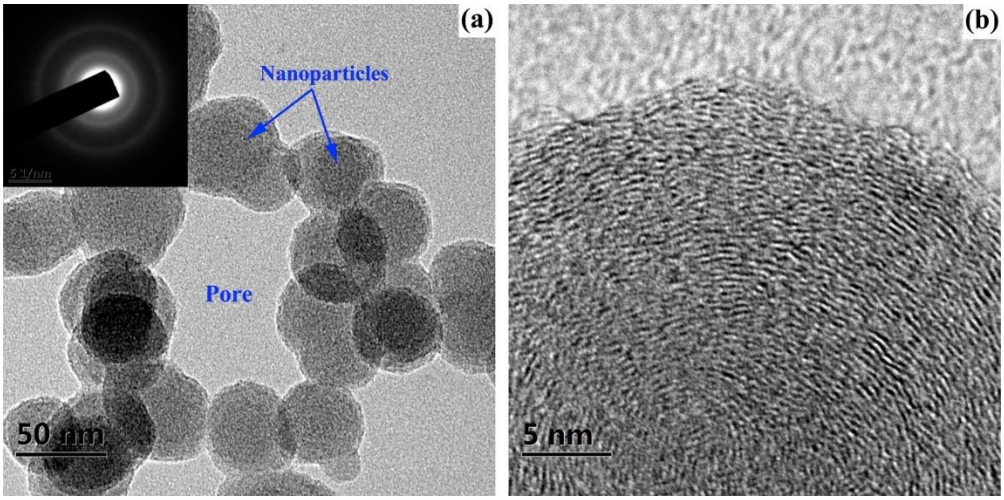

Figure **2** (a) TEM and SAED images and (b) the corresponding HR-TEM image of the amorphous nanoporous structure of a catalyst synthesized via electrochemical dealloying of $Pd_{32}Ni_{48}P_{20}$ alloy at 0.85 V in 0.5 M H_2SO_4 electrolyte. Reprinted from reference [87] with permission from Intermetallics. Copyright (2017) of Intermetallics

Even though XRD has certain limitations when it comes to characterizing amorphous nanoparticles as mentioned above, it is still the easiest and most conventional tool used to study the amorphous structure of materials. Therefore, it is often used for rapid evaluation, helping to investigate the influence of various factors, such as composition and temperature, on the amorphous structure. An amorphous structure is characterized by a long-range disorder of the metal lattice. Therefore, characteristic sharp peaks of a crystal structure are not present in XRD spectra of amorphous Pt or Pd.

Amorphous structure is the result of mixing additional elements into the lattice of noble metal. Each element contributes to amorphousness differently and a critical concentration of an element is crucial in engineering amorphous catalysts. For bulk metal alloys, the interaction of metals in the mixture is the key to achieve amorphous phase. The phases of the metals can be evaluated by using a phase diagram. For dealloyed Pd-based amorphous alloys, interaction between Pd and Cu creates a fixing effect, preventing the metal atoms from diffusing and recrystallizing during dealloying [85, 86]. For P-doped nanocatalysts, when metals and non-metal P that are used for alloying and doping, respectively, are introduced into the lattice, they induce a lattice disorder, which is the key to induce amorphous structure. It has been reported that P is the main factor that disorders the lattice [103]. When the P content increases, the crystal structure becomes more disordered and eventually turns amorphous. On the other hand, metals such as transition metals Cu and Ni that are used for alloying cause the lattice to contract. While providing an opposite effect compared to that of P, they are believed to enhance thermal stability of amorphous catalysts. Due to the opposing effects, the concentration of each element plays a key role in ensuring that the final material is amorphous. According to reported studies, for systems containing Cu, scientists have found out that Cu content must be kept below 20 at% [104]. Meanwhile for systems containing Ni, a minimum concentration of 15 at% of P is required to achieve amorphous structure for Pd [87]. For systems without any metal used for alloying, atomic concentration of P can still be lower (11%) while amorphous structure is still achieved [76]. In the case of Pt, while the critical concentration for obtaining amorphous structure is not discussed, the atomic percent of P follows a similar pattern to that in Pd catalysts. For example, 34 at% of P, i.e.,., atomic ratio of Pt/P is 2:1, was reported for amorphous PtP/C [105], 49 at% of P for PtNiP/C [102], and 37 at% P or an atomic ratio of roughly 1:3 Pt/P for PtNiRuP/C [66].

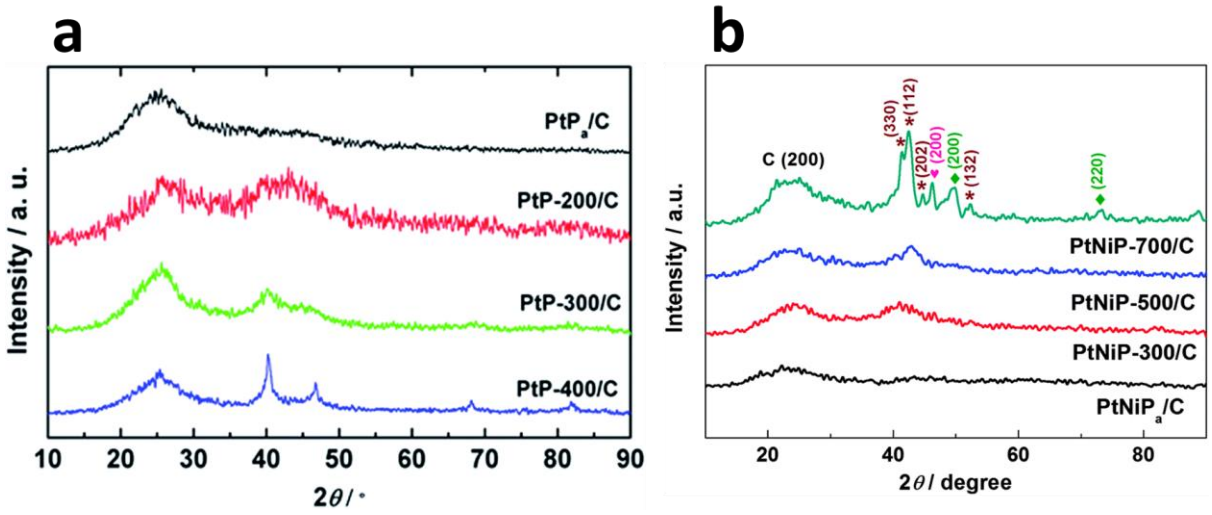

Figure **3** XRD spectra of: (a) PtP/C catalysts annealed at different temperatures. Reprinted from reference [105] with permission from RSC Advances. Copyright (2014) of RSC Advances. (b) PtNiP/C catalysts annealed at different temperatures. Reprinted from reference [102] with permission from PCCP. Copyright (2014) of PCCP

The thermal stabilization effect of alloyed transition metal has been observed in P-doped Pt-based amorphous catalysts. Amorphous PtP/C catalyst reported by Ma et al. [105] started to recrystallize when annealed at 200°C and fully transitioned into a crystalline structure at 400°C (Fig. 3a). When Ni was introduced into the PtNiP/C catalyst reported by the same group [102], the catalyst only started to recrystallize at 300°C and only turned into a crystalline structure at 700°C (Fig. 3b). Although there is no study on crystallinity evolution of PdP system for a clear comparison, PdNiP has been reported to be stable up to 350°C. The effect of concentration of metals used for alloying to thermal stability of the catalyst is not investigated in detail, but generally, 300°C should be a safe processing temperature for these catalysts.

3.2. Size and shape

The shapes of amorphous catalysts are not very diverse. Many of the synthesis methods only use simple surfactants to achieve the desired shape. In an amorphous structure, there is no preferred growth direction, so the shape of amorphous catalysts is confined by the surfactant in use. Most often seen shapes are spheres.

Some works reported amorphous nanocatalysts synthesized in the presence of surfactants, which greatly affects the size distribution of the catalyst. Zhao et al. [106] investigated different surfactants and reactants for the synthesis of monodisperse Pd-Ni-P nanoparticles as seen in Fig. 4. The conditions are summarized in Table 1. From the figure, only the optimal condition could yield a monodisperse distribution: palladium acetylacetonate [$Pd(acac)_2$, 0.2 mmol], nickel acetylacetonate [$Ni(acac)_2$, 0.6 mmol], and triphenylphosphine (TPP, 1.76 mmol) as Pd, Ni, and P sources, respectively; tetra-*n*-butylammonium bromide (TBAB, 2 mmol) and trioctylphosphine oxide (TOPO, 6 mmol) as surfactants; and oleylamine (OLA, 12 mL) as a reducing reagent and a stabilizer.

Table 1 Optimizing conditions for the fabrication of monodisperse amorphous Pd-Ni-P NPs

Pd source	Ni source	P source	Surfactant	Reductant and stabilizer	Sample
$Pd(acac)_2$	$Ni(acac)_2$	PPh_3	TBAB/TOPO	OLA/OA	1
$Pd(acac)_2$	$Ni(acac)_2$	PPh_3	–	OLA	2
$Pd(acac)_2$	$Ni(acac)_2$	TOP	–	OLA	3
$Pd(acac)_2$	$Ni(acac)_2$	PPh_3	TBAB/TOPO	OLA	4

Data are reproduced from [106] with permission from Chemistry of Materials. Copyright (2014) of Chemistry of Materials

PPh_3 triphenylphosphine

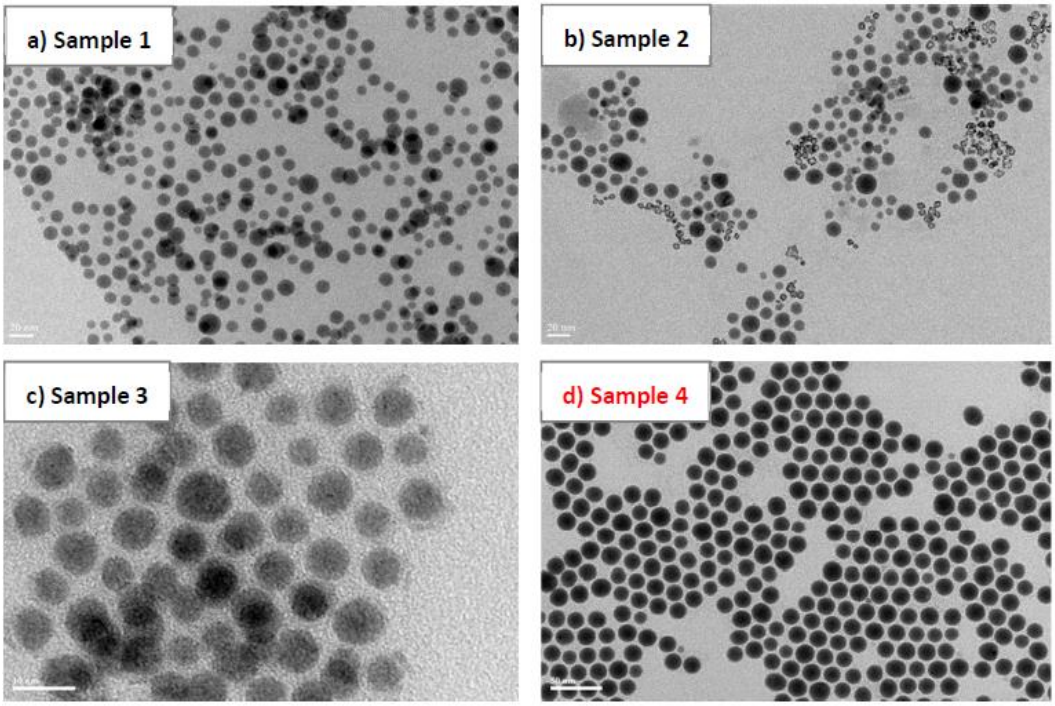

Figure **4** TEM images of Pd-Ni-P NPs obtained from different reaction conditions summarized in Table 1. Reprinted from reference [106] with permission from Chemistry of Materials. Copyright (2014) of Chemistry of Materials

In the syntheses of the majority of amophous catalysts, surfactants are not ultilized. As a result, the size distribution of the catalysts follows a normal distrbution, as exemplified in Fig. 5, where the amorphous PtNiP nanoparticles subjected to various temperatures for thermal treatment are depicted.

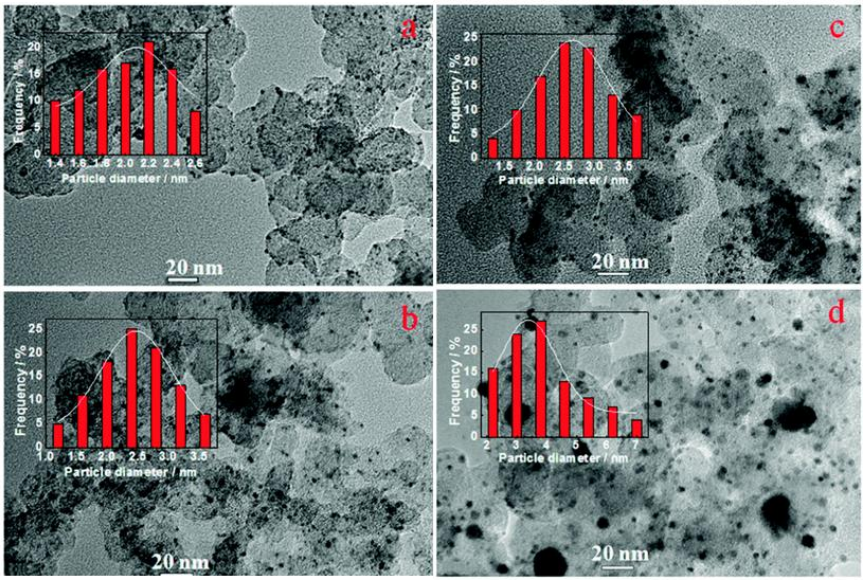

Figure **5**. TEM images and corresponding histograms of PtNiP particle size distribution (*insets*) of amorphous PtNiP/C catalyst (a) and PtNiP/C catalysts annealed at different temperatures: PtNiP-300/C (b), PtNiP-500/C (c), and PtNiP-700/C (d). Reprinted from reference [102] with permission from PCCP. Copyright (2014) of PCCP

For catalysts synthesized without a shape-determining surfactant, the size-reduction effect of P can be observed as illustrated in Fig. 6. Using the stepwise electroless deposition method reported by Poon et al. [76], the use of NaH_2PO_2 as a reducing agent yielded P-doped amorphous Pd nanoparticles with a visibly smaller particle size compared to the crystalline counterpart reduced by N_2H_4. Size-reduction effect in P-doped nanoparticles was investigated by Daimon et al. [107]. This reduction in size greatly contributes to the superior mass activity of these amorphous catalysts, which is of high importance as Pt and Pd are costly noble metals.

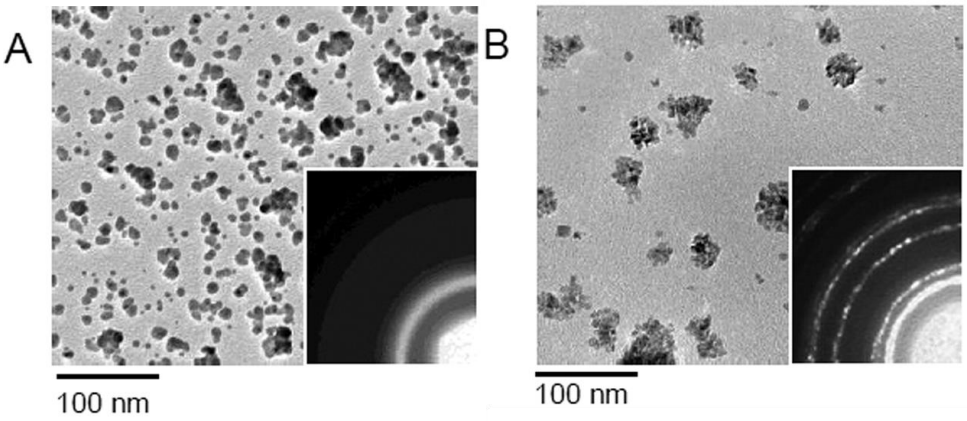

Figure **6** TEM and SAED images of Pd nanoparticles synthesized by stepwise electroless deposition process using (a) NaH_2PO_2 and (b) N_2H_4 as reducing agents. Reprinted from reference [76] with permission from the Journal of the American Chemical Society. Copyright (2014) of the Journal of the American Chemical Society

With the recent discovery of ligand-exchange method, more shapes can be achieved depending on the original surfactant used, as exemplified in Fig. 7 [99]. An ultrathin Pd nanosheet synthesized using octanoic acid as a capping agent [108] (Fig. 7a) can be transformed into amorphous structure (Fig. 7b) while maintaining its shape [109]. Similarly, Pd nanocubes synthesized using poly(vinylpyrrolidone) [110] (Fig. 7c) could be transformed to amorphous nanocubes (Fig. 7d) via ligand exchange with bismuthiol I.

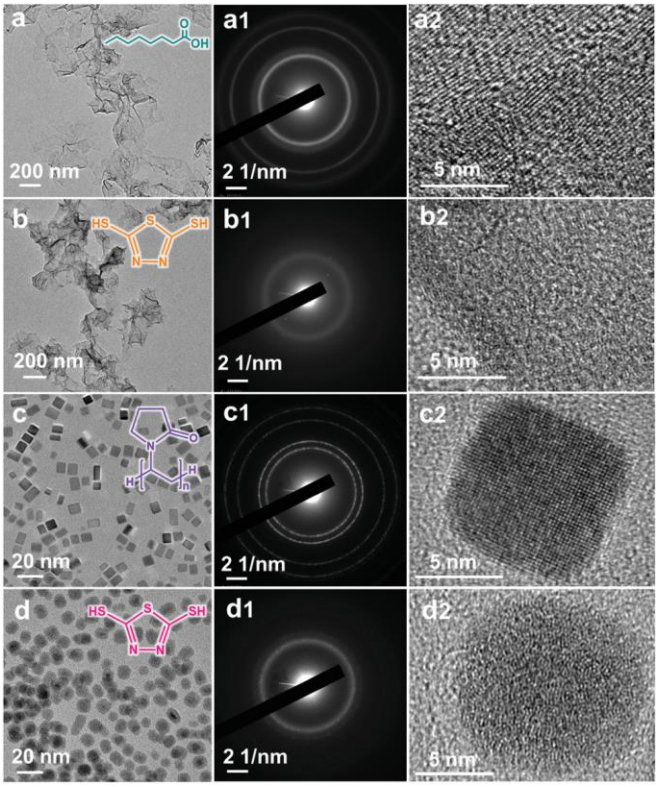

Figure **7** (*a*) TEM, (*a1*) SAED, and (*a2*) HR-TEM images of Pd nanosheet with octanoic acid as a capping agent (OA). *Inset* in *a* is the molecular structure of OA. (*b*) TEM, (*b1*) SAED, and (b2) HR-TEM images of Pd nanosheet synthesized via ligand exchange with bismuthiol I for 24 h. *Inset* in *b* is the molecular structure of bismuthiol I. (*c*) TEM, (*c1*) SAED, and (*c2*) HR-TEM images of Pd nanocubes synthesized using poly(vinylpyrrolidone (PVP)). *Inset* in *c* is the molecular structure of PVP. (*d*) TEM, (*d1*) SAED, and (*d2*) HR-TEM images of Pd nanocubes via ligand exchange with bismuthiol I for 24 h. *Inset* in *d* is the molecular structure of bismuthiol I. Reprinted from reference [99] with permission from Advanced Materials. Copyright (2020) of Advanced Materials

3.3. XPS study

When additional elements are introduced into a lattice, the bonding and electronic structure will change. XPS is used to investigate these changes.

3.3.1. P-doped nanocatalysts

In P-doped nanocatalysts, the interaction between P atoms and noble metal Pt and Pd atoms is evident and is often carefully investigated. P is an electronegative element that might withdraw electrons from Pt and Pd, resulting in a decreased electron density in these noble metals, which is beneficial for catalytic activity.

In PdP systems, the Pd 3*d* peaks often can be deconvoluted into two pairs of doublets: $3d_{5/2}$ and $3d_{3/2}$ levels of metallic Pd^0 and $3d_{5/2}$ and $3d_{3/2}$ of oxidation state Pd^{2+} as shown in Fig. 8. Across all reported systems of PdP, peaks corresponding to $3d_{5/2}$ and $3d_{3/2}$ levels of Pd^0 range from 335.2 to 335.6 eV and from 340.5 to 340.8 eV, respectively, while $3d_{5/2}$ and $3d_{3/2}$ peaks of Pd^{2+} range from 335.7 to 337.5 eV and from 341.4 to 342.7 eV, respectively. Comparing the peak position of $3d_{5/2}$ of Pd^0 for PdP to that for pure Pd, there is a slight shift in binding energy. This indicates that there is electron transfer from Pd to P, leaving Pd positively charged [6, 72, 111, 112]. In the PdNiP systems, interestingly, the binding energy of $3d_{5/2}$ of Pd^0 is much higher at 337.8 eV, exhibiting a much more dramatic shift of more than 2 eV [106, 113].

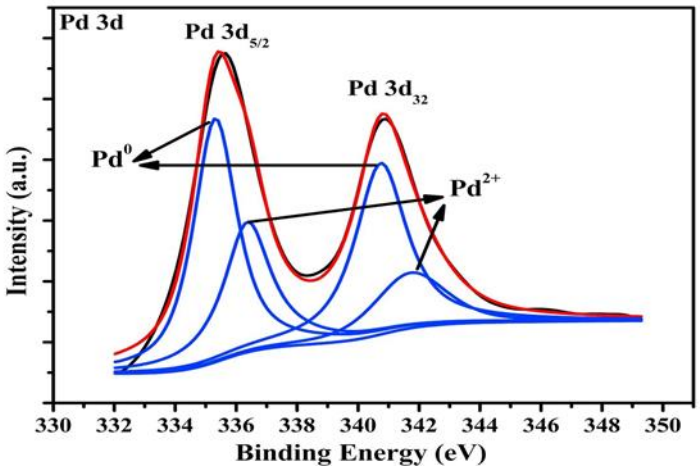

Figure **8** Pd 3*d* XPS spectrum of amorphous PdP nanoparticles. Reprinted from reference [112] with permission from Applied Surface Science. Copyright (2018) of Applied Surface Science

P is an element with many valence states; therefore, it is expected to exist in different forms and species in the metal lattices. There are numerous factors that determine what species should be present and their relative concentration in the catalysts, which may include support materials, synthesis method, and influences from other components. For PdP synthesized on carbon nanospheres using wet reduction method reported by Zhao et al. [112], the P 2*p* spectra can be fitted to multipeaks of different oxidation states. The fitted P $2p_{3/2}$ peak at 132.7 eV represented P that bonds to one or two oxygen atoms [114]. The peak at 129.6 eV (P $2p_{1/2}$) is elemental phosphorous [115], and the most intense doublet at 133.7 eV corresponds to P $2p_{1/2}$ of phosphates. The peaks at 134.8 and 136.0 eV can be attributed to P=O and P_2O_5, respectively [112, 114, 115]. The type of P species present also depends on the concentration of P in the lattice. According to Salomé et al. [6], the catalyst $PdP_{10}t_3$ with 10 at% of P synthesized by electrodeposition has phosphorus in one single form, i.e.,., alloyed with Pd, while $PdP_{15}t_3$ synthesized using the same electrodeposition technique but has higher P concentration of 15 at%, shows the presence of oxidized phosphorus as phosphate groups besides PdP. Similarly, Zhang et al. [111] synthesized Pd/P NP networks using wet reduction method. The P 2*p* peaks at 129.5 and 134.3 eV correspond to elemental state phosphorus P^0 and oxidized phosphorus P^v, respectively. Compared to the XPS data of bulk P from research [116, 117], the binding energy of P shifts negatively. The shifts in binding energy of P in the PdP NP networks further confirm the electronic interactions between Pd and P, resulting in electron transfer from Pd to electronegative P [111, 116, 118].

For Pt-based catalysts, Pt 4*f* XPS spectra have two peaks corresponding to Pt $4f_{7/2}$ and Pt $4f_{5/2}$ states. These peaks can be deconvoluted into three pairs of doublets corresponding to metallic Pt^0 and oxidized states Pt^{II} and Pt^{IV}, as shown in Fig. 9. For Pt-based catalysts, the binding energy of Pt 4*f* shifts positively, similar to that for Pd-based catalysts but in contrary to that of Pt/C catalyst due the donation of electrons from Pt to P. As mentioned above, Pt exists in both metallic and oxidized states. However, the ratio is different across different systems. For PtP, Pt is predominantly in oxidized states [105]. For PtNiRuP, Pt exists mainly in metallic state [66], while PtNiP has a balanced mix of both metallic and oxidized states [102, 119, 120].

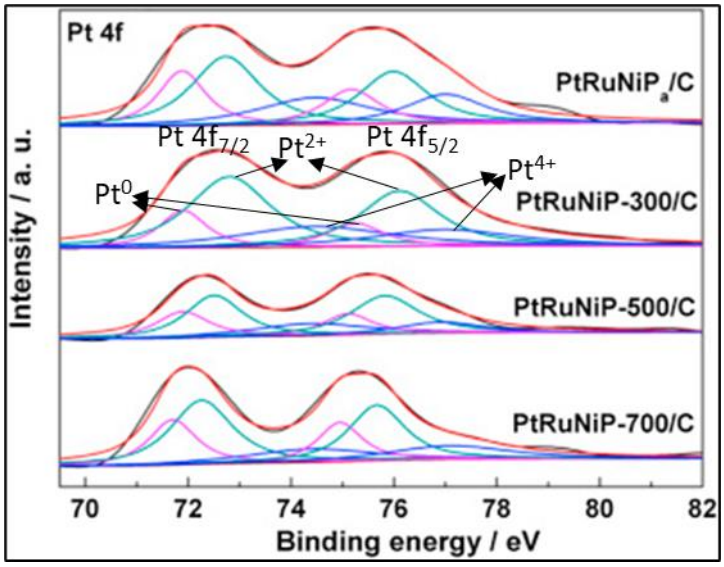

Figure **9** Pt 4*f* spectra of PtRuNiP/C nanoparticles annealed at different temperatures. Reproduced from [66] with permission from the Journal of Power Sources. Copyright (2014) of the Journal of Power Sources

XPS peaks of P in Pt-based catalysts also exhibit a negative shift in a similar manner to that in Pd-based catalysts, owing to the fact that P donates electrons to Pt. P 2*p* peak can be fitted into two individual component peaks at 133.4–133.6 eV and at 134.4–134.8 eV, corresponding to P^{III} and P^{V}, respectively [118, 121, 122].

3.3.2. Dealloyed Pd-based amorphous alloys

In dealloyed Pd-based amorphous alloys, S is doped as a result of the dealloying process. Being an electronegative element much like P, an electron transfer interaction is also expected and often investigated.

Pd peaks also experience a similar positive shift in binding energy, as seen in Fig. 10, owing to the fact that the S doped into the lattice is also a highly electronegative element with many valence states similar to P. Peaks corresponding to $3d_{5/2}$ and $3d_{3/2}$ levels of Pd^0 range from 336.2 to 336.6 eV and from 341.6 to 341.8 eV, while $3d_{5/2}$ and $3d_{3/2}$ peaks of Pd^{2+} range from 337.3 to 337.5 eV and from 342.5 to 342.6 eV. Comparing the peak position of $3d_{5/2}$ of Pd^0 to that for pure Pd, there is a larger shift in binding energy compared to that for pure Pd [85, 86].

In the spectra of S 2*p*, there are often two pairs of doublets: the higher binding energy doublet for bridging S_2^{2-} and/or apical S^{2-} and the lower binding energy doublet for terminal S_2^{2-} and/or S^{2-} in the materials. There are also peaks attributed to SO_4^{2-} residue from dealloying process. It has been reported that bridging S_2^{2-} and/or apical S^{2-} on surface of catalyst might contribute to improve catalytic activity [85, 86].

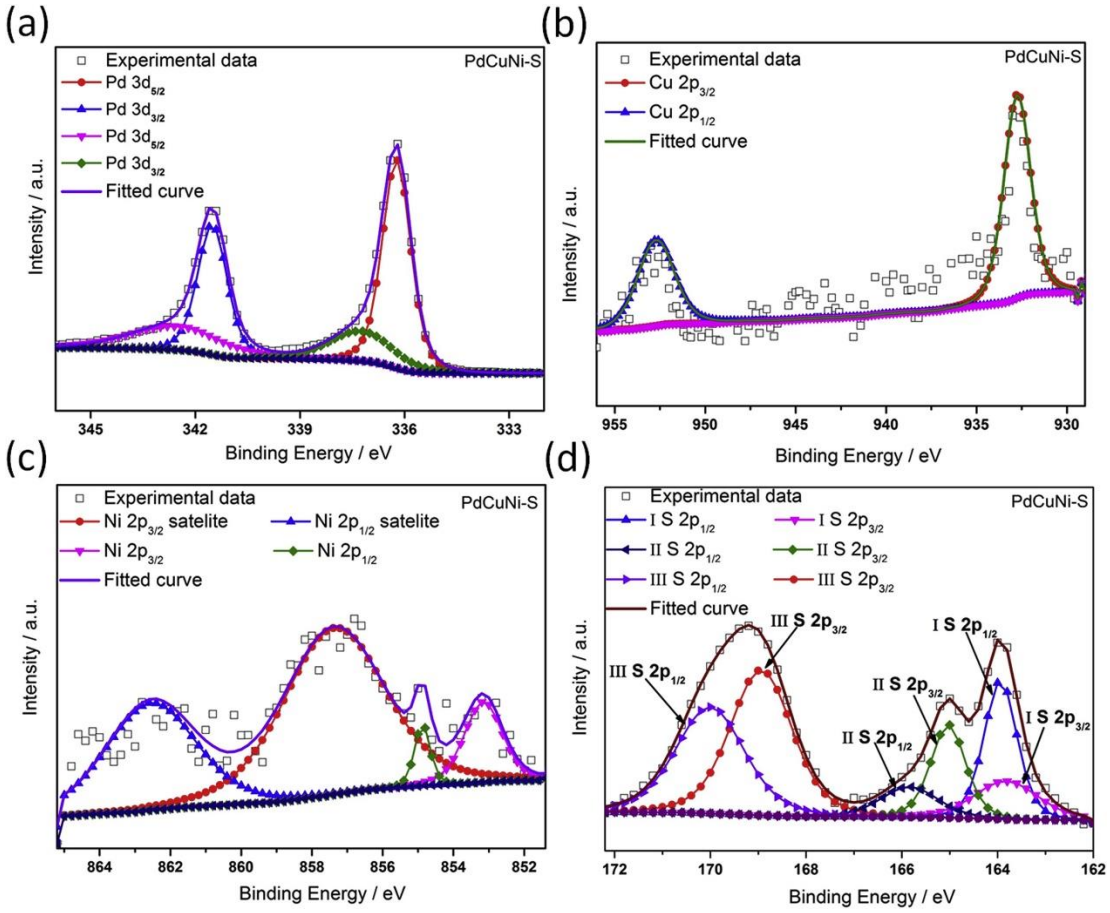

Figure **10**. XPS spectra of (a) Pd 3*d*, (b) Cu 2*p*, (c) Ni 2*p*, and (d) S 2*p* of PdCuNi–S catalyst. Reprinted from reference [86] with permission from Applied Catalysis B: Environmental. Copyright (2019) of Applied Catalysis B: Environmental

4. Electrocatalytic activity

Oxygen reduction reaction (ORR), formic acid oxidation (FAO), and methanol/ethanol oxidation reactions (EOR/MOR) are important fuel cell reactions. Unfortunately, they have sluggish kinetics and high susceptibility to catalyst poisoning [4, 116, 123-136]. Therefore, a significant amount of research has been conducted to design catalysts that can overcome these challenges. Catalysts with amorphous structure has shown a great promise through many successful reports. Amorphous structure is characterized by a long-range disorder that gives rise to low-coordination active sites. These sites are responsible for the improvement in the activity of catalysts with amorphous structures [75, 76] in comparison to their crystalline forms. Low-coordination active sites (kinks, edges and steps) have been experimentally proved by previous fundamental studies to be the active sites where bonds scission occurs [137-142]. Theoretical investigation has suggested that atoms in the neighborhood of surface irregularities experience profound chemical effects such as energy level rearrangement and charge transfer, which resulted in increased density of states and appearance of bonding orbitals which are not available in flat surfaces, are believed to contribute to their enhanced reactivities [143-145]. In this section, catalytic activity of amorphous catalysts is discussed in comparison to that of their crystalline counterparts.

4.1. Anode reactions

Anode reactions of fuel cells comprise of many small organic molecules electro-oxidation such as methanol oxidation or formic acid oxidation. They often suffer from CO poisoning, which is a reaction intermediate that binds strongly to active sites and deactivates them. Interestingly, amorphous catalysts possess better CO tolerance than their crystalline counterpart, resulting in higher durability besides their higher current density output. As mentioned above in the XPS data discussion, binding energies of Pt and Pd often experience a positive shift, which translates to weaker bonding to poisoning species and consequentially higher poisoning resistance and durability. Besides the effect of electron transfer from electronegative elements such as P and S inside the lattice of these catalysts, Richter et al. also proposed, via experimental and theoretical analysis, that the shift can also be attributed to lattice strain [146].

4.1.1. Methanol oxidation reaction

Methanol oxidation is known for its importance as an anode reaction in fuel cells. Methanol is a popular fuel because of its ease of transportation and storage, low operating temperature, and high-energy density [147-152].

In an experiment by Wang et al. [87], PdNiP was fabricated by electrodealloying. The amorphous PdNiP was dealloyed at a lower potential of 0.85 V while the crystalline counterpart was dealloyed at 0.88 V. In Fig. 11, the cyclic voltammetry (CV) measurements of the two catalysts revealed that the amorphous PdNiP (denoted NP-A) is 1.5 times more efficient than its crystalline counterpart (denoted NP-B) in terms of specific activity (1.31 versus 0.82 mA cm^{-2}). The durability of the catalyst was also briefly investigated with 100 CV cycles, which resulted in only a slight current reduction of 9%. There are various explanations on why amorphous structure can increase the activity of catalysts. Amorphous structure has many active sites arising from the high amount of lattice defects, which can promote catalytic activity. The abundance of surface atoms with unsaturated coordination provided more active sites for reactions [153, 154]. Hu et al. [155] substantiated this claim by demonstrating using density functional theory calculations that atoms are bonded differently in amorphous structure compared to crystalline one.

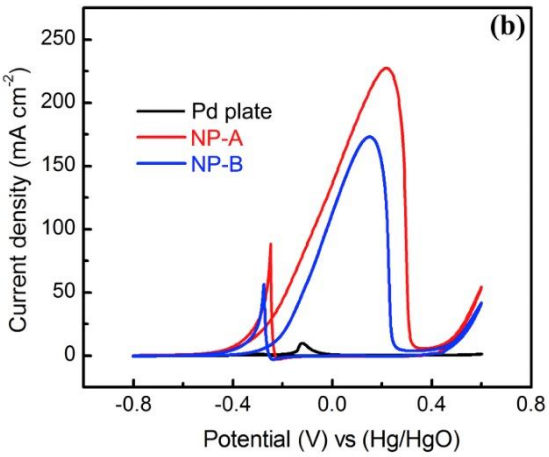

Figure **11** CV curves of pure Pd plate, sample NP-A, and sample NP-B in 1.0 M KOH and 1.0 M methanol solution. Scan rate was 20 mV s^{-1}. Reprinted from reference [87] with permission from Intermetallics. Copyright (2017) of Intermetallic

Annealing test is another approach to confirm the effect of amorphous structure on catalytic activity. In the study done by Zhao et al. [113], annealing at 400°C converts the amorphous Pd-Ni-P/CNT catalysts into their crystalline forms. In a similar manner, the catalytic activity decreases as can be

seen in Fig. 12. The high catalytic activity is attributed to the random nature in the arrangement of Pd, Ni, and P atoms as well as the electron deficiency of Pd (indicated by the positive shift in binding energy of Pd $3d_{5/2}$ observed via XPS). The electron deficiency is believed to weaken the adsorption of reaction intermediates of MOR into Pd, therefore improving the catalytic activity of the amorphous Pd-Ni-P/CNT [156, 157].

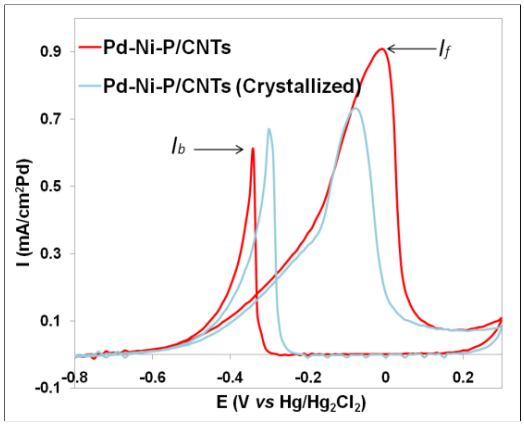

Figure **12** Current density–potential curves of the cyclic voltammetry measurements carried out to compare the MOR catalytic activities of amorphous and crystallized Pd-Ni-P/CNTs. Reprinted from reference [87] with permission from the International Journal of Electrochemical Science. Copyright (2016) of the International Journal of Electrochemical Science

Another study by Zhao et al. [106] sought to investigate the durability of amorphous Pd-Ni-P/C nanoparticles in greater details, as shown in Fig. 13. After 400 cycles in an electrolyte solution containing methanol, the catalytic activity of Pd-Ni-P/C only dropped by 3.5% compared to a drastic 45% decrease in commercial Pd catalyst. Similarly, after 300 cycles, ECSA still remained up to 91.4% of the maximum values. Such durability is attributed to the combination of Pd and NiO, in addition to other common factors such as abundance of uncoordinated active sites due to the amorphous structure and Pd electron deficiency [156-159].

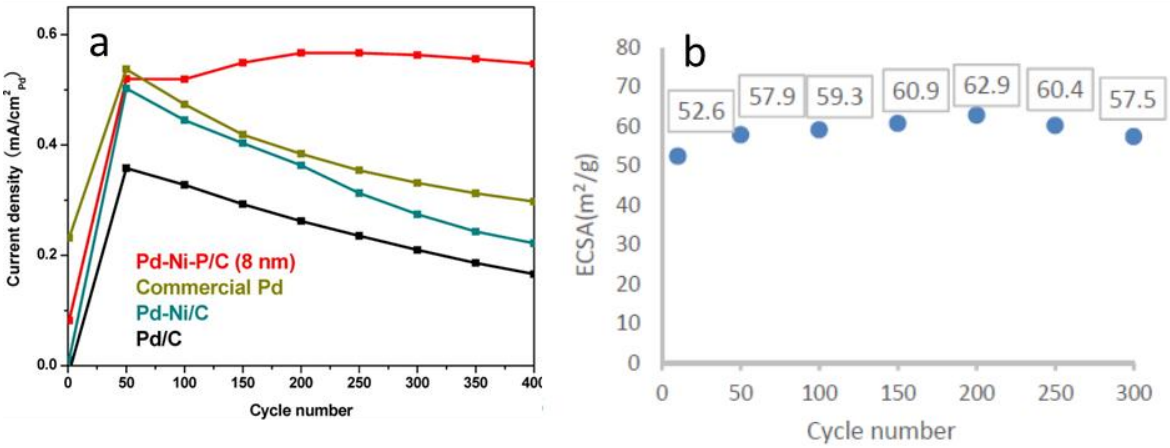

Figure **13** (a) Time–current density function of CV-monitored MOR using different Pd-based catalysts. The maximum current density measured during every anodic scan as a function of cycle number is given. (b) ECSA values calculated from cyclic CV tests of 8-nm Pd-Ni-P/C that are carried out in deaerated 0.5 M KOH. Reprinted from reference [106] with permission from Chemistry of Materials. Copyright (2014) of Chemistry of Materials

In the case of amorphous Pt-based catalysts for MOR such PtP/C [105] and PtNiP/C [102] developed by Ma et al., their phase transition induced by heat treatment (annealing at various temperatures)

was investigated in greater details. The overall trend shows that amorphous catalysts have the most superior performance: highest current density, most negative onset potential for CV, and highest current retention for chronoamperometry. These parameters gradually degrade as the catalysts transition into their crystalline form at a higher temperature. This trend can be observed clearly in Fig. 14 with PtP/C as an example.

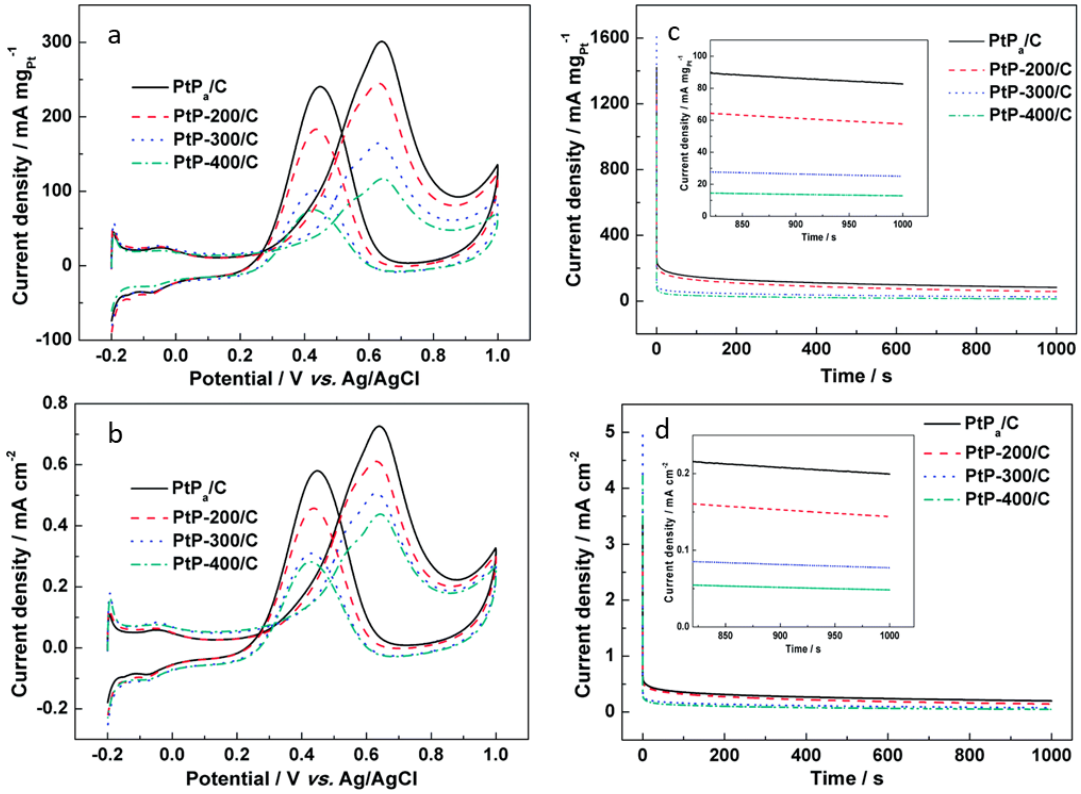

Figure **14** CV graphs from measurement done in 0.5 M H_2SO_4 + 0.5 M CH_3OH at a scan rate of 50 mV s^{-1}. Measurements were normalized by (a) Pt loading and (b) ECSA derived from CO stripping ($ECSA_{CO}$). Chronoamperometry curves obtained by measurements at a potential of 0.6 V in 0.5 M H_2SO_4 + 0.5 M CH_3OH were normalized by (c) Pt loading and (d) $ECSA_{CO}$ of four catalysts: amorphous PtP supported on carbon (amorphous PtP/C) and PtP supported on carbon annealed at 200°C, 300°C, and 400°C (PtP-200/C, PtP-300/C, and PtP-400/C, respectively). Reprinted from reference [105] with permission from RSC Advances. Copyright (2014) of RSC Advances

Other amorphous Pt-based catalysts, such as the amorphous CuPt synthesized via $Na_2S_2O_3$-mediated galvanic displacement reported by Zhao et al. [160], also displayed a similar difference in catalytic activity between amorphous and crystalline forms. Amorphous CuPt has a higher specific activity, more negative onset potential, and higher cyclic stability compared to both crystalline CuPt (synthesized via non-mediated galvanic displacement) and commercial Pt/C, as shown in Fig. 15.

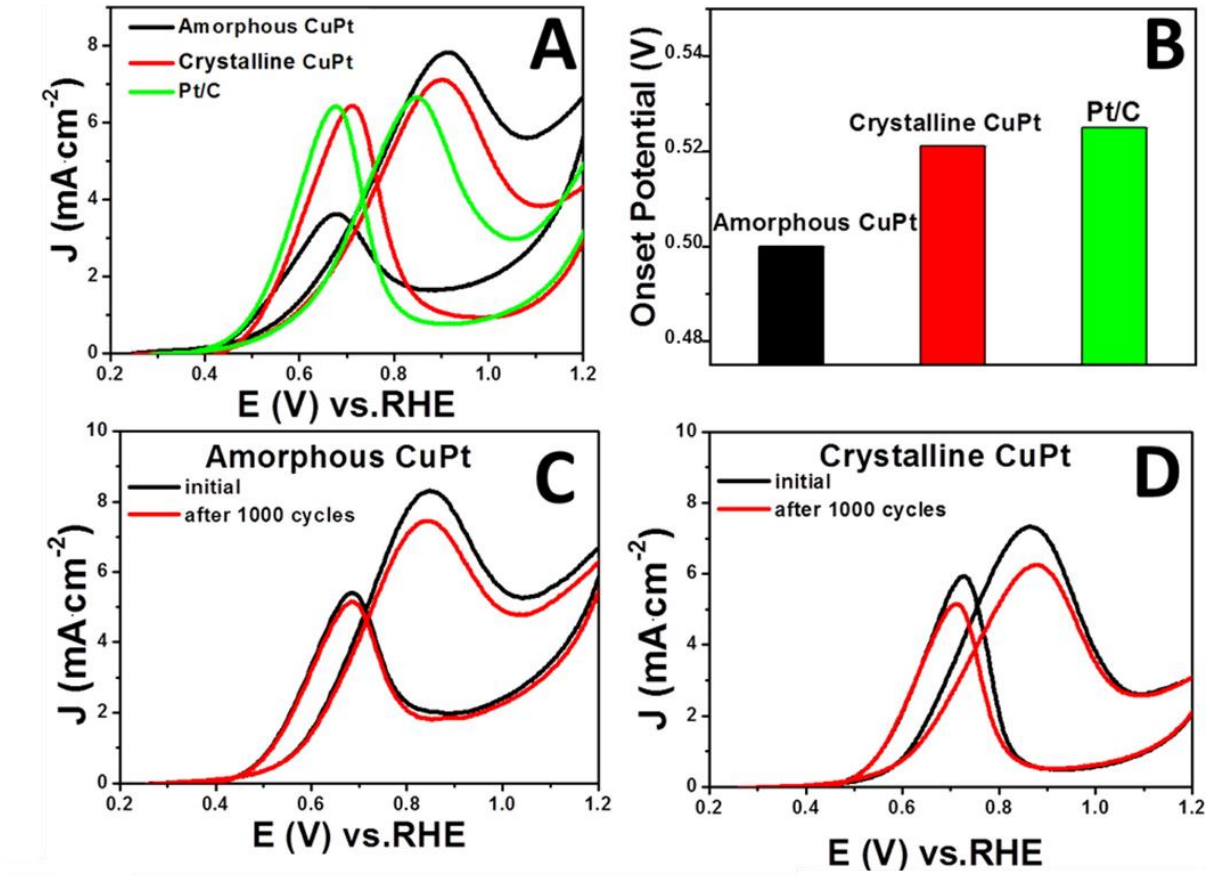

Figure **15** (a) CV curves from measurements run in N_2-saturated 0.1 M $HClO_4$ and 0.5 M CH_3OH solution at a scan rate of 10 mV s^{-1}. (b) Onset potentials. Long-term stability measurements: CV curves of (c) amorphous CuPt and (d) crystalline CuPt before and after 1,000 cycles. Reprinted from reference [160] with permission from ACS Catalysis. Copyright (2016) of ACS Catalysis

4.1.2. Formic acid oxidation

Formic acid oxidation is also one of the popular anode reactions of fuel cells because formic acid is a fuel with high performance, is environmentally friendly, and most importantly has low crossover rate [59, 161-164].

The amorphous Pd-P catalyst synthesized via facile stepwise electroless deposition reported by Poon et al. [75] was investigated for its catalytic capability for FAO. The number of cycles carried out during synthesis could fine-tune the P content of the catalyst, affecting the level of lattice disorder that ultimately influences its catalytic activity. Nonetheless, all variations of reported amorphous Pd-P catalysts that follow the desirable dehydrogenation pathway display higher specific and mass activities than commercial Pd/C, which can be seen in Fig. 16a, b. They also have higher durability (Fig. 16c). Annealing test was again used to prove the contribution of the amorphous the structure to the catalytic activity, with results shown in Fig. 16d.

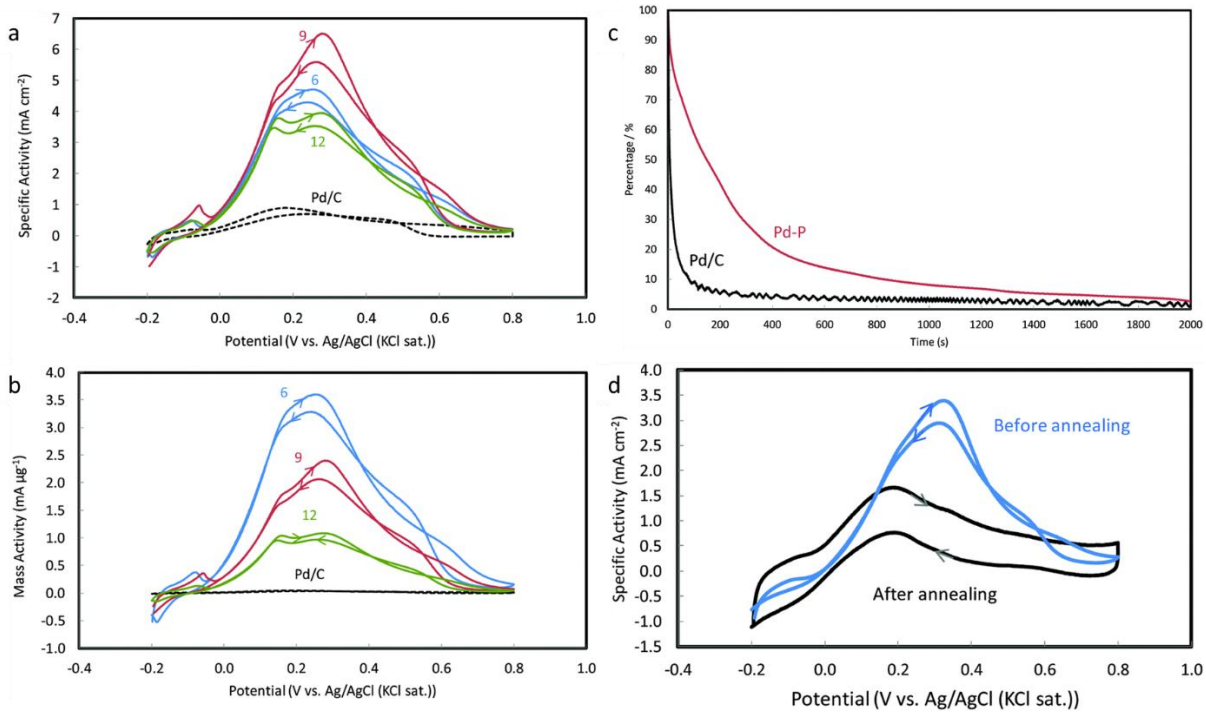

Figure **16** (a) Specific activity and (b) mass activity graphs of Pd-P NPs and Pd/C from CV measurements done in N_2-saturated 0.5 M H_2SO_4 + 1 M HCOOH solution at a scan rate is 50 mV s^{-1}. The number beside the curves denotes the number of deposition cycles. (c) Chronoamperometry results for Pd-P and Pd/C, which were evaluated as a percentage of initial current density. Measurements were performed in N_2-saturated 0.5 M H_2SO_4 + 1 M HCOOH solution at a potential of 0.2 V versus Ag/AgCl (KCl saturated). (d) Specific activity graphs (six cycles) of Pd-P NPs deposited on a carbon cloth before and after annealing at 700°C for 1 h. CV measurements were performed in N_2-saturated 0.5 M H_2SO_4 + 1 M HCOOH solution at a scan rate of 50 mV s^{-1}. Reprinted from reference [75] with permission from Chemical Communications. Copyright (2016) of Chemical Communications

Zhang et al. [165] reported a porous Pd (P-Pd) nanosheet synthesized via reduction by CO, which has an amorphous–crystalline heterostructure. The amorphous–crystalline heterostructure increases the number of active sites, which in turn improved the catalytic activity of the nanosheet. It has higher specific activity and mass activity as well as durability compared to commercially available Pd/C, as seen in Fig. 17.

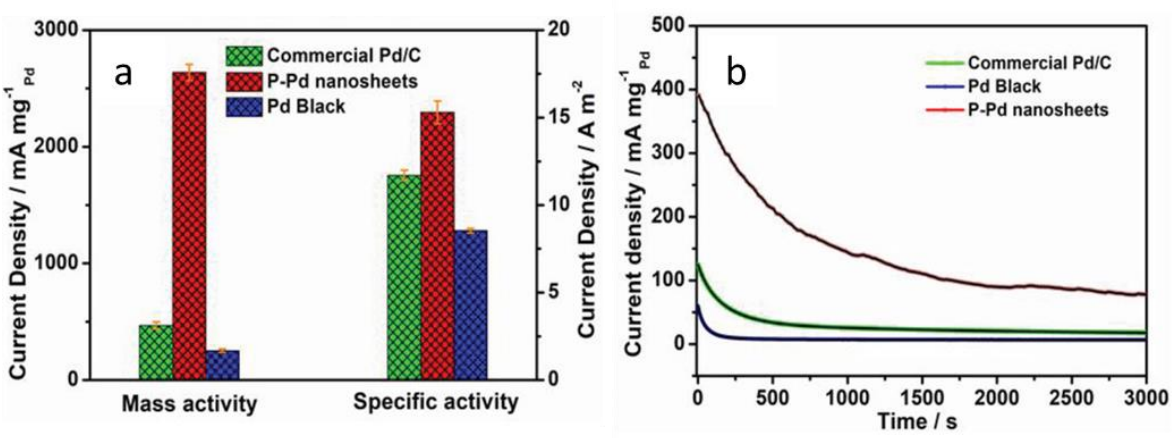

Figure **17** (a) Activities and (b) chronoamperometry curves of various Pd-based catalysts based on measurements performed in 0.5 M H_2SO_4 + 0.5 M HCOOH solution. Reprinted from reference [165] with permission from Small. Copyright (2019) of Small

4.2. Cathode reaction—oxygen reduction reaction

Oxygen reduction reaction is an important cathodic reaction in fuel cells [76, 166, 167].

A superior amorphous Pd-P catalyst reported by Poon et al. [76] has higher catalytic activity and durability than commercial Pd/C and even Pt/C for ORR, as can be seen in Fig. 18. There is a remarkable positive shift in the ORR curves experienced by the amorphous Pd-P catalysts. Interestingly, the catalytic activity can be fine-tuned simply by varying the number of cycles of deposition. The Pd-P catalyst was also subjected to annealing at 700°C for 1 h. The annealed Pd-P catalyst experienced a dramatic drop in its catalytic activity, exhibiting almost the same ORR curve as its crystalline Pd–N_2H_4 counterpart (reduced by N_2H_4). The annealing test result again showed that the contributing factor to high catalytic activity is the amorphous structure. The amorphous Pd-P catalyst also has superior durability compared to their commercial counterparts, as evident from the 30,000-s chronoamperometry test result.

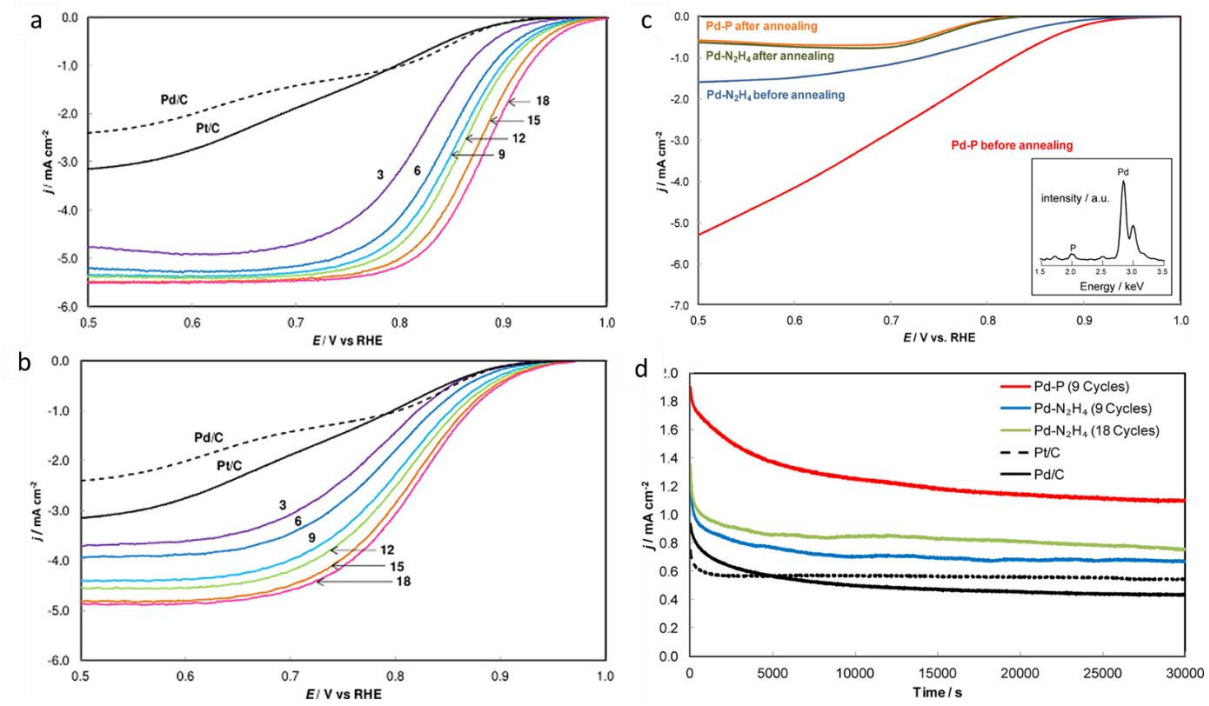

Figure **18**. ORR polarization curves for Pd nanoparticles synthesized with (a) NaH_2PO_2 and (b) N_2H_4. Measurements were performed in O_2-saturated 0.1 M KOH solution at a scan rate of 10 mV s^{-1} and a rotational speed of 1,600 rpm. The numbers beside the curves correspond to the cycle numbers of the stepwise electroless deposition process. (c) ORR polarization curves of Pd nanoparticles synthesized on a carbon cloth. Annealing was performed at 700°C for 1 h. *Inset* is the EDS spectra of Pd-P after the annealing, indicating that P remains even after the annealing. (d) Chronoamperometry response of Pd nanoparticles synthesized with NaH_2PO_2 or N_2H_4 and performed in O_2-saturated 0.1 M KOH solution at potential of 0.666 V versus reference hydrogen electrode (RHE) and a rotational speed of 200 rpm. Reprinted from reference [76] with permission from the Journal of the American Chemical Society. Copyright (2014) of the Journal of the American Chemical Society

Ma et al. [120] reported an amorphous PtNiP/C catalyst for ORR as well. Koutecky–Levich calculations revealed that its synthesis followed a four-electron electron transfer pathway, reducing O_2 to H_2O. The amorphous catalyst was also heat treated at 500°C for hour to obtain its crystalline form for comparison. It is clear in Fig. 19 that the crystalline catalyst has a more inferior catalytic activity, as indicated by the negative shift in its ORR curve and lower specific activity and mass activity values at 0.6 and 0.65 V.

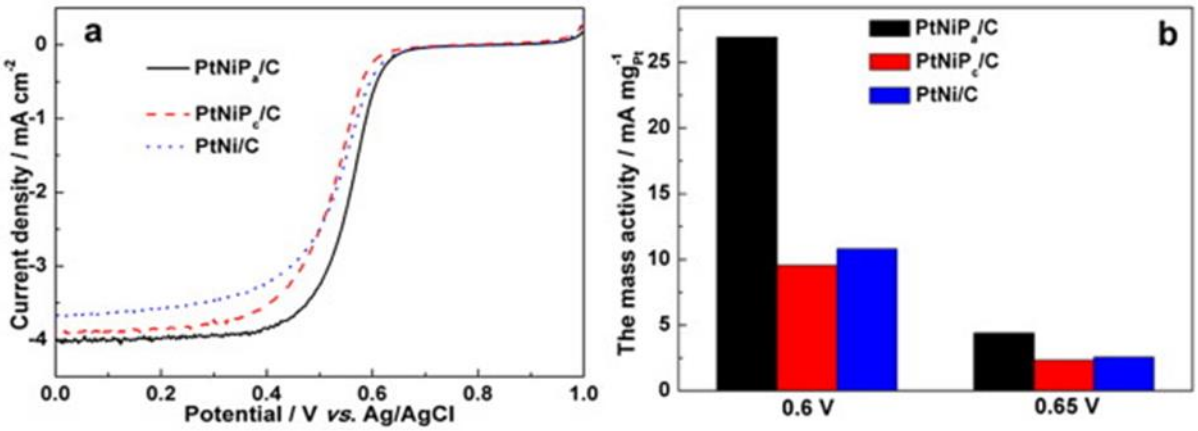

Figure **19** (a) ORR polarization curves of amorphous PtNiP/C, crystalline PtNiP/C, and PtNi/C catalysts for oxygen reduction in O_2-saturated 0.5 M H_2SO_4 solution at a scan rate of 5 mV s^{-1} and rotation speed of 1,600 rpm. (b) Mass activity of amorphous PtNiP/C, crystalline PtNiP/C, and PtNi/C catalysts at 0.60 and 0.65 V. Reprinted from reference [120] with permission from the Journal of Power Sources. Copyright (2014) of the Journal of Power Sources

5. Conclusion and future prospects

Amorphous structure is a promising approach in the design of effective catalysts for fuel cell applications. In this review, synthesis methods, properties, and catalytic activity of amorphous Pt- and Pd-based catalysts have been systematically discussed. Many synthesis methods have been developed to synthesize noble-metal-based amorphous catalysts with increasingly smaller size and higher performance, each with their own unique strength and practicality. The superior catalytic activities of these amorphous catalysts can be attributed to the abundance of uncoordinated active sites as the result of a characteristic long-range disordered structure. In addition, the elements introduced into the lattice to induce amorphous structure, via doping and alloying, also change the electronic structure of Pt and Pd, which helps increase their performance.

Even though utilizing amorphous structure is a breakthrough in catalyst science thanks to its unique properties, there are still much room for improvement. Looking at the trend across literature reporting on amorphous Pt- and Pd-based catalysts, it is suggested that more works should be done to validate the applicability of the catalysts in fuel cells and improve the catalysts further.

First, it is noticed that the studies for different fuel cell reactions of amorphous Pt- and Pd-based catalysts have not been conducted in good proportion. Majority of the catalysts reported are tested for MOR, while reports on FAO or ORR applications are relatively sparse. It is proposed that more amorphous Pt- and Pd-based catalysts should be synthesized and tested for more diverse fuel cell reactions other than MOR. This could prove the versatility of these amorphous catalysts and provide deeper and broader understanding on their catalytic activity.

Second, despite the promising results reported, the structural stability of these amorphous catalysts is overlooked. Amorphous structure is a metastable state hence it easily undergoes structural relaxation. Harsh operating conditions of fuel cells can potentially destabilize these catalysts and cause them to recrystallize. Therefore, future research on amorphous catalysts should address their long-term stability. Possible strategies are to either increase the number of elements used in the alloys or introduce novel functionalized support [102, 168, 169].

Lastly, the electrochemical tests carried out to prove the superior catalytic activity of these materials are just “proof of concept.” The transition from half-cell reaction test to full-cell test is often met by various challenges. It is encouraged that testing in full-cell setup be carried out so that the difficulties

in applying these promising amorphous Pt- and Pd-based nanocatalysts to fuel cells can be fully understood, addressed, and resolved.

Acknowledgements

This work is supported by the Singapore Ministry of Education [MOE2017-T2-2-067] and NTUitive [NGF-2018-05-017]. The authors thank Ms. Koh Joo Luang, Ms. Yong Mei Yoke, Mr. Leong Kwok Phui and Mr. Roger Tan Kay Chia at NTU, for their constant support with maintaining excellent experimental environments.

References

1. Kirubakaran, A., S. Jain, and R.K. Nema, *A review on fuel cell technologies and power electronic interface.* Renewable and Sustainable Energy Reviews, 2009. **13**(9): p. 2430-2440 DOI: https://doi.org/10.1016/j.rser.2009.04.004.
2. Peighambardoust, S.J., S. Rowshanzamir, and M. Amjadi, *Review of the proton exchange membranes for fuel cell applications.* Int. J. Hydrogen Energy, 2010. **35**(17): p. 9349-9384 DOI: https://doi.org/10.1016/j.ijhydene.2010.05.017.
3. Zhang, J., *PEM fuel cell electrocatalysts and catalyst layers: fundamentals and applications*. 2008: Springer Science & Business Media.
4. Gewirth, A.A. and M.S. Thorum, *Electroreduction of Dioxygen for Fuel-Cell Applications: Materials and Challenges.* Inorg. Chem., 2010. **49**(8): p. 3557-3566 DOI: 10.1021/ic9022486.
5. Rabis, A., P. Rodriguez, and T.J. Schmidt, *Electrocatalysis for Polymer Electrolyte Fuel Cells: Recent Achievements and Future Challenges.* ACS Catalysis, 2012. **2**(5): p. 864-890 DOI: 10.1021/cs3000864.
6. Salomé, S., et al., *Synthesis and testing of new carbon-supported PdP catalysts for oxygen reduction reaction in polymer electrolyte fuel cells.* J. Electroanal. Chem., 2015. **754**: p. 8-21
7. Lefèvre, M., et al., *Iron-based catalysts with improved oxygen reduction activity in polymer electrolyte fuel cells.* Science, 2009. **324**(5923): p. 71-74
8. Yeager, E., *Electrocatalysts for O2 reduction.* Electrochim. Acta, 1984. **29**(11): p. 1527-1537 DOI: https://doi.org/10.1016/0013-4686(84)85006-9.
9. Liu, H., et al., *High-surface-area CoTMPP/C synthesized by ultrasonic spray pyrolysis for PEM fuel cell electrocatalysts.* Electrochim. Acta, 2007. **52**(13): p. 4532-4538 DOI: https://doi.org/10.1016/j.electacta.2006.12.056.
10. Liang, H.-W., et al., *Mesoporous Metal–Nitrogen-Doped Carbon Electrocatalysts for Highly Efficient Oxygen Reduction Reaction.* J. Am. Chem. Soc., 2013. **135**(43): p. 16002-16005 DOI: 10.1021/ja407552k.
11. Kattel, S. and G. Wang, *Reaction Pathway for Oxygen Reduction on FeN4 Embedded Graphene.* The Journal of Physical Chemistry Letters, 2014. **5**(3): p. 452-456 DOI: 10.1021/jz402717r.
12. Hu, Y., et al., *Hollow Spheres of Iron Carbide Nanoparticles Encased in Graphitic Layers as Oxygen Reduction Catalysts.* Angew. Chem. Int. Ed., 2014. **53**(14): p. 3675-3679 DOI: 10.1002/anie.201400358.
13. Zhu, H., et al., *Monodisperse MxFe3–xO4 (M = Fe, Cu, Co, Mn) Nanoparticles and Their Electrocatalysis for Oxygen Reduction Reaction.* Nano Lett., 2013. **13**(6): p. 2947-2951 DOI: 10.1021/nl401325u.
14. Zhang, Y., et al., *Manganese dioxide-coated carbon nanotubes as an improved cathodic catalyst for oxygen reduction in a microbial fuel cell.* J. Power Sources, 2011. **196**(22): p. 9284-9289 DOI: https://doi.org/10.1016/j.jpowsour.2011.07.069.

15. Shi, Q., et al., *Sulfur and nitrogen co-doped carbon nanotubes for enhancing electrochemical oxygen reduction activity in acidic and alkaline media.* Journal of Materials Chemistry A, 2013. **1**(47): p. 14853-14857 DOI: 10.1039/C3TA12647A.
16. Liang, Y., et al., *Oxygen Reduction Electrocatalyst Based on Strongly Coupled Cobalt Oxide Nanocrystals and Carbon Nanotubes.* J. Am. Chem. Soc., 2012. **134**(38): p. 15849-15857 DOI: 10.1021/ja305623m.
17. Cheng, F., et al., *Enhancing Electrocatalytic Oxygen Reduction on MnO2 with Vacancies.* Angew. Chem. Int. Ed., 2013. **52**(9): p. 2474-2477 DOI: 10.1002/anie.201208582.
18. Zheng, Y., et al., *Two-Step Boron and Nitrogen Doping in Graphene for Enhanced Synergistic Catalysis.* Angew. Chem. Int. Ed., 2013. **52**(11): p. 3110-3116 DOI: 10.1002/anie.201209548.
19. Wong, C.H.A., et al., *Graphene Oxide Nanoribbons from the Oxidative Opening of Carbon Nanotubes Retain Electrochemically Active Metallic Impurities.* Angew. Chem. Int. Ed., 2013. **52**(33): p. 8685-8688 DOI: 10.1002/anie.201303837.
20. Su, P., et al., *Nitrogen-doped carbon nanotubes derived from Zn–Fe-ZIF nanospheres and their application as efficient oxygen reduction electrocatalysts with in situ generated iron species.* Chemical Science, 2013. **4**(7): p. 2941-2946 DOI: 10.1039/C3SC51052B.
21. Liu, R., et al., *Nitrogen-Doped Ordered Mesoporous Graphitic Arrays with High Electrocatalytic Activity for Oxygen Reduction.* Angew. Chem. Int. Ed., 2010. **49**(14): p. 2565-2569 DOI: 10.1002/anie.200907289.
22. Ding, W., et al., *Space-Confinement-Induced Synthesis of Pyridinic- and Pyrrolic-Nitrogen-Doped Graphene for the Catalysis of Oxygen Reduction.* Angew. Chem. Int. Ed., 2013. **52**(45): p. 11755-11759 DOI: 10.1002/anie.201303924.
23. Chen, P., et al., *Nitrogen-doped nanoporous carbon nanosheets derived from plant biomass: an efficient catalyst for oxygen reduction reaction.* Energy & Environmental Science, 2014. **7**(12): p. 4095-4103 DOI: 10.1039/C4EE02531H.
24. Nie, Y., L. Li, and Z. Wei, *Recent advancements in Pt and Pt-free catalysts for oxygen reduction reaction.* Chem. Soc. Rev., 2015. **44**(8): p. 2168-2201 DOI: 10.1039/C4CS00484A.
25. Ge, X., et al., *Oxygen Reduction in Alkaline Media: From Mechanisms to Recent Advances of Catalysts.* ACS Catalysis, 2015. **5**(8): p. 4643-4667 DOI: 10.1021/acscatal.5b00524.
26. Oezaslan, M., F. Hasché, and P. Strasser, *PtCu3, PtCu and Pt3Cu Alloy Nanoparticle Electrocatalysts for Oxygen Reduction Reaction in Alkaline and Acidic Media.* J. Electrochem. Soc., 2012. **159**(4): p. B444-B454 DOI: 10.1149/2.106204jes.
27. Iwasita, T., *Methanol and CO electrooxidation*, in *Handbook of Fuel Cells – Fundamentals, Technology and Applications*, A.L. W. Vielstich, H.A. Gasteiger and H.Yokokawa, Editor. 2010, John Wiley & Sons, Ltd.
28. Beden, B., *Electrosorption of methanol on a platinum electrode. IR spectroscopic evidence for adsorbed CO species.* 1981
29. Deng, K., et al., *Pt–Ni–P nanocages with surface porosity as efficient bifunctional electrocatalysts for oxygen reduction and methanol oxidation.* Journal of Materials Chemistry A, 2019. **7**(16): p. 9791-9797 DOI: 10.1039/C9TA00928K.
30. Gong, W., et al., *Cross-double dumbbell-like Pt–Ni nanostructures with enhanced catalytic performance toward the reactions of oxygen reduction and methanol oxidation.* Applied Catalysis B: Environmental, 2019. **246**: p. 277-283 DOI: https://doi.org/10.1016/j.apcatb.2019.01.061.
31. Fang, C., et al., *AuPt Bipyramid Nanoframes as Multifunctional Platforms for In Situ Monitoring of the Reduction of Nitrobenzene and Enhanced Electrocatalytic Methanol Oxidation.* Chemistry – A European Journal, 2019. **25**(30): p. 7351-7358 DOI: 10.1002/chem.201900403.
32. Kim, K.S., et al., *Ultrathin-Polyaniline-Coated Pt–Ni Alloy Nanooctahedra for the Electrochemical Methanol Oxidation Reaction.* Chemistry – A European Journal, 2019. **25**(29): p. 7185-7190 DOI: 10.1002/chem.201900238.

33. Huang, L., et al., *Shape-Control of Pt–Ru Nanocrystals: Tuning Surface Structure for Enhanced Electrocatalytic Methanol Oxidation.* J. Am. Chem. Soc., 2018. **140**(3): p. 1142-1147 DOI: 10.1021/jacs.7b12353.
34. Xia, B.Y., et al., *One-Pot Synthesis of Cubic PtCu3 Nanocages with Enhanced Electrocatalytic Activity for the Methanol Oxidation Reaction.* J. Am. Chem. Soc., 2012. **134**(34): p. 13934-13937 DOI: 10.1021/ja3051662.
35. Li, C., et al., *Emerging Pt-based electrocatalysts with highly open nanoarchitectures for boosting oxygen reduction reaction.* Nano Today, 2018. **21**: p. 91-105
36. Li, C., et al., *Electrochemical deposition: an advanced approach for templated synthesis of nanoporous metal architectures.* Acc. Chem. Res., 2018. **51**(8): p. 1764-1773
37. Jiang, B., et al., *Mesoporous metallic iridium nanosheets.* J. Am. Chem. Soc., 2018. **140**(39): p. 12434-12441
38. Li, C., et al., *Pore-tuning to boost the electrocatalytic activity of polymeric micelle-templated mesoporous Pd nanoparticles.* Chemical science, 2019. **10**(14): p. 4054-4061
39. Garrick, T.R., et al., *The Effect of the Surface Composition of Ru-Pt Bimetallic Catalysts for Methanol Oxidation.* Electrochim. Acta, 2016. **195**: p. 106-111 DOI: https://doi.org/10.1016/j.electacta.2016.02.134.
40. Cui, Z., et al., *Synthesis of Structurally Ordered Pt3Ti and Pt3V Nanoparticles as Methanol Oxidation Catalysts.* J. Am. Chem. Soc., 2014. **136**(29): p. 10206-10209 DOI: 10.1021/ja504573a.
41. Sun, J., et al., *Carbon nanotubes supported Pt-Co-P ultrafine nanoparticle electrocatalysts with superior activity and stability for methanol electro-oxidation.* Electrochim. Acta, 2016. **215**: p. 447-454 DOI: https://doi.org/10.1016/j.electacta.2016.08.133.
42. Yan, X., et al., *Well dispersed Pt–Pd bimetallic nanoparticles on functionalized graphene as excellent electro-catalyst towards electro-oxidation of methanol.* J. Electroanal. Chem., 2016. **770**: p. 33-38 DOI: https://doi.org/10.1016/j.jelechem.2016.03.033.
43. Xiao, Y., et al., *Increasing Pt methanol oxidation reaction activity and durability with a titanium molybdenum nitride catalyst support.* J. Power Sources, 2015. **273**: p. 33-40 DOI: https://doi.org/10.1016/j.jpowsour.2014.09.057.
44. Xiao, Y., et al., *Robust non-carbon titanium nitride nanotubes supported Pt catalyst with enhanced catalytic activity and durability for methanol oxidation reaction.* Electrochim. Acta, 2014. **141**: p. 279-285 DOI: https://doi.org/10.1016/j.electacta.2014.07.070.
45. Huang, S.-Y., P. Ganesan, and B.N. Popov, *Electrocatalytic Activity and Stability of Titania-Supported Platinum–Palladium Electrocatalysts for Polymer Electrolyte Membrane Fuel Cell.* ACS Catalysis, 2012. **2**(5): p. 825-831 DOI: 10.1021/cs300088n.
46. Liu, Y. and W.E. Mustain, *High Stability, High Activity Pt/ITO Oxygen Reduction Electrocatalysts.* J. Am. Chem. Soc., 2013. **135**(2): p. 530-533 DOI: 10.1021/ja307635r.
47. Hong, T.-Z., et al., *Great-enhanced performance of Pt nanoparticles by the unique carbon quantum dot/reduced graphene oxide hybrid supports towards methanol electrochemical oxidation.* J. Power Sources, 2016. **303**: p. 109-117 DOI: https://doi.org/10.1016/j.jpowsour.2015.10.092.
48. Bu, L., et al., *Biaxially strained PtPb/Pt core/shell nanoplate boosts oxygen reduction catalysis.* Science, 2016. **354**(6318): p. 1410 DOI: 10.1126/science.aah6133.
49. Jin, H., et al., *Emerging Two-Dimensional Nanomaterials for Electrocatalysis.* Chem. Rev., 2018. **118**(13): p. 6337-6408 DOI: 10.1021/acs.chemrev.7b00689.
50. Chen, Y., et al., *Two-Dimensional Metal Nanomaterials: Synthesis, Properties, and Applications.* Chem. Rev., 2018. **118**(13): p. 6409-6455 DOI: 10.1021/acs.chemrev.7b00727.
51. Jiang, K., et al., *Efficient oxygen reduction catalysis by subnanometer Pt alloy nanowires.* Science Advances, 2017. **3**(2): p. e1601705 DOI: 10.1126/sciadv.1601705.

52. Yan, X., et al., *Triangular AgAu@Pt core–shell nanoframes with a dendritic Pt shell and enhanced electrocatalytic performance toward the methanol oxidation reaction.* Nanoscale, 2018. **10**(5): p. 2231-2235 DOI: 10.1039/C7NR08899J.
53. Zhang, Z., et al., *One-Pot Synthesis of Highly Anisotropic Five-Fold-Twinned PtCu Nanoframes Used as a Bifunctional Electrocatalyst for Oxygen Reduction and Methanol Oxidation.* Adv. Mater., 2016. **28**(39): p. 8712-8717 DOI: 10.1002/adma.201603075.
54. Bai, Z., et al., *A Facile Preparation of Hollow Palladium Nanosphere Catalysts for Direct Formic Acid Fuel Cell.* The Journal of Physical Chemistry C, 2009. **113**(24): p. 10568-10573 DOI: 10.1021/jp902713k.
55. Guo, S., S. Dong, and E. Wang, *A General Method for the Rapid Synthesis of Hollow Metallic or Bimetallic Nanoelectrocatalysts with Urchinlike Morphology.* Chemistry – A European Journal, 2008. **14**(15): p. 4689-4695 DOI: 10.1002/chem.200800077.
56. Liang, H.-P., et al., *Pt Hollow Nanospheres: Facile Synthesis and Enhanced Electrocatalysts.* Angew. Chem. Int. Ed., 2004. **43**(12): p. 1540-1543 DOI: 10.1002/anie.200352956.
57. Zhao, J., et al., *Novel carbon supported hollow Pt nanospheres for methanol electrooxidation.* J. Power Sources, 2006. **162**(1): p. 168-172 DOI: https://doi.org/10.1016/j.jpowsour.2006.06.090.
58. Jiang, B., et al., *Mesoporous Pt nanospheres with designed pore surface as highly active electrocatalyst.* Chemical Science, 2016. **7**(2): p. 1575-1581 DOI: 10.1039/C5SC03779D.
59. Chen, L., et al., *Nanoporous PdNi bimetallic catalyst with enhanced electrocatalytic performances for electro -oxidation and oxygen reduction reactions.* Adv. Funct. Mater., 2011. **21**(22): p. 4364-4370
60. Ding, L.-X., et al., *Porous Pt-Ni-P Composite Nanotube Arrays: Highly Electroactive and Durable Catalysts for Methanol Electrooxidation.* J. Am. Chem. Soc., 2012. **134**(13): p. 5730-5733 DOI: 10.1021/ja212206m.
61. Hoster, H., et al., *Current-Time Behavior of Smooth and Porous PtRu Surfaces for Methanol Oxidation.* J. Electrochem. Soc., 2001. **148**(5): p. A496 DOI: 10.1149/1.1365142.
62. Lv, H., et al., *Mesoporous palladium–boron alloy nanospheres.* Journal of Materials Chemistry A, 2019. **7**(43): p. 24877-24883 DOI: 10.1039/C9TA09822D.
63. Xiong, L. and A. Manthiram, *Nanostructured Pt–M/C (M=Fe and Co) catalysts prepared by a microemulsion method for oxygen reduction in proton exchange membrane fuel cells.* Electrochim. Acta, 2005. **50**(11): p. 2323-2329 DOI: https://doi.org/10.1016/j.electacta.2004.10.046.
64. Wittkopf, J.A., J. Zheng, and Y. Yan, *High-Performance Dealloyed PtCu/CuNW Oxygen Reduction Reaction Catalyst for Proton Exchange Membrane Fuel Cells.* ACS Catalysis, 2014. **4**(9): p. 3145-3151 DOI: 10.1021/cs500692y.
65. Barroso, J., et al., *Trimetallic amorphous catalyst with low amount of platinum: Comparative study for ethanol, bioethanol and CO electrooxidation.* Int. J. Hydrogen Energy, 2014. **39**(8): p. 3984-3990 DOI: https://doi.org/10.1016/j.ijhydene.2013.05.168.
66. Ma, Y., et al., *Evolution of the electrocatalytic activity of carbon-supported amorphous platinum–ruthenium–nickel–phosphorous nanoparticles for methanol oxidation.* J. Power Sources, 2014. **268**: p. 498-507 DOI: https://doi.org/10.1016/j.jpowsour.2014.06.091.
67. Yu, W., M.D. Porosoff, and J.G. Chen, *Review of Pt-Based Bimetallic Catalysis: From Model Surfaces to Supported Catalysts.* Chem. Rev., 2012. **112**(11): p. 5780-5817 DOI: 10.1021/cr300096b.
68. Beyhan, S., J.-M. Léger, and F. Kadırgan, *Understanding the influence of Ni, Co, Rh and Pd addition to PtSn/C catalyst for the oxidation of ethanol by in situ Fourier transform infrared spectroscopy.* Applied Catalysis B: Environmental, 2014. **144**: p. 66-74 DOI: https://doi.org/10.1016/j.apcatb.2013.07.020.

69. Erini, N., et al., *Exceptional Activity of a Pt–Rh–Ni Ternary Nanostructured Catalyst for the Electrochemical Oxidation of Ethanol.* ChemElectroChem, 2015. **2**(6): p. 903-908 DOI: https://doi.org/10.1002/celc.201402390.
70. Li, R., et al., *Ultrasonic-assisted synthesis of Pd–Ni alloy catalysts supported on multi-walled carbon nanotubes for formic acid electrooxidation.* Electrochim. Acta, 2011. **56**(19): p. 6860-6865 DOI: https://doi.org/10.1016/j.electacta.2011.05.097.
71. Shi, Q., et al., *Synthesis of open-mouthed, yolk–shell Au@AgPd nanoparticles with access to interior surfaces for enhanced electrocatalysis.* Chemical Science, 2015. **6**(7): p. 4350-4357 DOI: 10.1039/C5SC01088H.
72. Yu, W., et al., *The role of surface functionalities in fabricating supported Pd-P nanoparticles for efficient formic acid oxidation.* Chem. Phys. Lett., 2017. **686**: p. 155-160
73. Hanifah, M.F.R., et al., *One-pot synthesis of efficient reduced graphene oxide supported binary Pt-Pd alloy nanoparticles as superior electro-catalyst and its electro-catalytic performance toward methanol electro-oxidation reaction in direct methanol fuel cell.* J. Alloys Compd., 2019. **793**: p. 232-246 DOI: https://doi.org/10.1016/j.jallcom.2019.04.114.
74. Qu, L., et al., *Nitrogen-Doped Graphene as Efficient Metal-Free Electrocatalyst for Oxygen Reduction in Fuel Cells.* ACS Nano, 2010. **4**(3): p. 1321-1326 DOI: 10.1021/nn901850u.
75. Poon, K.C., et al., *A highly active Pd–P nanoparticle electrocatalyst for enhanced formic acid oxidation synthesized via stepwise electroless deposition.* Chem. Commun., 2016. **52**(17): p. 3556-3559 DOI: 10.1039/C5CC08669H.
76. Poon, K.C., et al., *Newly Developed Stepwise Electroless Deposition Enables a Remarkably Facile Synthesis of Highly Active and Stable Amorphous Pd Nanoparticle Electrocatalysts for Oxygen Reduction Reaction.* J. Am. Chem. Soc., 2014. **136**(14): p. 5217-5220 DOI: 10.1021/ja500275r.
77. Suryanarayana, C., *Mechanical alloying and milling.* Prog. Mater Sci., 2001. **46**(1): p. 1-184 DOI: https://doi.org/10.1016/S0079-6425(99)00010-9.
78. Bhadeshia, H., *Recrystallisation of practical mechanically alloyed iron-base and nickel-base superalloys.* Materials Science and Engineering: A, 1997. **223**(1-2): p. 64-77
79. Barranco, J. and A. Pierna, *On the enhancement of methanol and CO electro-oxidation by amorphous (NiNb) PtSnRu alloys versus bifunctional PtRu and PtSn alloys.* J. Non-Cryst. Solids, 2008. **354**(47-51): p. 5153-5155
80. Sánchez, M., et al., *Amorphous catalysts based on (NiNb) 99 (Pt XY) 1 for DAFC using ethanol and bioethanol as fuels.* Int. J. Hydrogen Energy, 2014. **39**(8): p. 3991-3996
81. Barroso, J., et al., *Trimetallic amorphous catalyst with low amount of platinum: Comparative study for ethanol, bioethanol and CO electrooxidation.* Int. J. Hydrogen Energy, 2014. **39**(8): p. 3984-3990
82. Kreysa, G. and B. Håkansson, *Electrocatalysis by amorphous metals of hydrogen and oxygen evolution in alkaline solution.* Journal of electroanalytical chemistry and interfacial electrochemistry, 1986. **201**(1): p. 61-83
83. Correia, A., et al., *Amorphous palladium-silicon alloys for the oxidation of formic acid and formaldehyde. A voltammetric investigation.* Journal of the Brazilian Chemical Society, 1999. **10**(6): p. 478-482
84. Takahashi, T., et al., *Hydrogenation of benzene over catalyst prepared from amorphous Pt-Zr alloy.* Materials transactions, 2001. **42**(8): p. 1599-1602
85. Xu, W., et al., *A highly efficient electrocatalyst based on amorphous Pd–Cu–S material for hydrogen evolution reaction.* Journal of Materials Chemistry A, 2017. **5**(35): p. 18793-18800 DOI: 10.1039/C7TA05314B.
86. Yang, X., et al., *An amorphous nanoporous PdCuNi-S hybrid electrocatalyst for highly efficient hydrogen production.* Applied Catalysis B: Environmental, 2019. **246**: p. 156-165 DOI: https://doi.org/10.1016/j.apcatb.2019.01.030.

87. Wang, S., et al., *Enhanced electro-catalytic performance of Pd-based amorphous nanoporous structure synthesized by dealloying Pd32Ni48P20 metallic glass.* Intermetallics, 2017. **87**: p. 6-12
88. Kumar, G., A. Desai, and J. Schroers, *Bulk Metallic Glass: The Smaller the Better.* Adv. Mater., 2011. **23**(4): p. 461-476 DOI: https://doi.org/10.1002/adma.201002148.
89. Liu, L., M. Hasan, and G. Kumar, *Metallic glass nanostructures: fabrication, properties, and applications.* Nanoscale, 2014. **6**(4): p. 2027-2036 DOI: 10.1039/C3NR05645G.
90. Hasan, M., J. Schroers, and G. Kumar, *Functionalization of Metallic Glasses through Hierarchical Patterning.* Nano Lett., 2015. **15**(2): p. 963-968 DOI: 10.1021/nl504694s.
91. Hasan, M. and G. Kumar, *High-throughput drawing and testing of metallic glass nanostructures.* Nanoscale, 2017. **9**(9): p. 3261-3268 DOI: 10.1039/C7NR00126F.
92. Sekol, R.C., et al., *Pd–Ni–Cu–P metallic glass nanowires for methanol and ethanol oxidation in alkaline media.* Int. J. Hydrogen Energy, 2013. **38**(26): p. 11248-11255 DOI: https://doi.org/10.1016/j.ijhydene.2013.06.017.
93. Carmo, M., et al., *Bulk Metallic Glass Nanowire Architecture for Electrochemical Applications.* ACS Nano, 2011. **5**(4): p. 2979-2983 DOI: 10.1021/nn200033c.
94. Li, J., et al., *Recent Advances in Metallic Glass Nanostructures: Synthesis Strategies and Electrocatalytic Applications.* Adv. Mater., 2019. **31**(7): p. 1802120 DOI: https://doi.org/10.1002/adma.201802120.
95. Doubek, G., et al., *Guided Evolution of Bulk Metallic Glass Nanostructures: A Platform for Designing 3D Electrocatalytic Surfaces.* Adv. Mater., 2016. **28**(10): p. 1940-1949 DOI: https://doi.org/10.1002/adma.201504504.
96. Rudnik, E. and J. Gorgosz, *The influence of maleic acid on the Co–P electroless deposition.* Surf. Coat. Technol., 2007. **201**(16): p. 6953-6959 DOI: https://doi.org/10.1016/j.surfcoat.2006.12.025.
97. Rudnik, E., K. Kokoszka, and J. Łapsa, *Comparative studies on the electroless deposition of Ni–P, Co–P and their composites with SiC particles.* Surf. Coat. Technol., 2008. **202**(12): p. 2584-2590 DOI: https://doi.org/10.1016/j.surfcoat.2007.09.026.
98. Podestá, J.J. and R.C.V. Piatti, *Amorphous Pd-P, Au-P and Co-P alloys as cathode materials in alkaline solution for oxygen reduction.* International Journal of Hydrogen Energy, 1997. **22**(8): p. 753-758 DOI: https://doi.org/10.1016/S0360-3199(96)00208-X.
99. Cheng, H., et al., *Ligand-Exchange-Induced Amorphization of Pd Nanomaterials for Highly Efficient Electrocatalytic Hydrogen Evolution Reaction.* Adv. Mater., 2020. **32**(11): p. 1902964 DOI: 10.1002/adma.201902964.
100. Tejos, M., et al., *Thin amorphous platinum films photochemically obtained, and their potential use as modified electrodes.* Thin Solid Films, 2002. **409**(2): p. 172-177 DOI: https://doi.org/10.1016/S0040-6090(02)00129-3.
101. Zhao, Y., et al., *Amorphous CuPt Alloy Nanotubes Induced by Na2S2O3 as Efficient Catalysts for the Methanol Oxidation Reaction.* ACS Catalysis, 2016. **6**: p. 4127-4134
102. Ma, Y., et al., *Evolution of nanoscale amorphous, crystalline and phase-segregated PtNiP nanoparticles and their electrocatalytic effect on methanol oxidation reaction.* PCCP, 2014. **16**(8): p. 3593-3602 DOI: 10.1039/C3CP54600D.
103. Lv, H., et al., *Ternary Palladium-Boron-Phosphorus Alloy Mesoporous Nanospheres for Highly Efficient Electrocatalysis.* ACS Nano, 2019. **13**(10): p. 12052-12061 DOI: 10.1021/acsnano.9b06339.
104. Zhao, M., et al., *Composition-Dependent Morphology of Bi-and Trimetallic Phosphides: Construction of Amorphous Pd–Cu–Ni–P Nanoparticles as a Selective and Versatile Catalyst.* ACS applied materials & interfaces, 2017. **9**(40): p. 34804-34811
105. Ma, Y., et al., *Synthesis of ultrafine amorphous PtP nanoparticles and the effect of PtP crystallinity on methanol oxidation.* RSC Advances, 2014. **4**(40): p. 20722-20728 DOI: 10.1039/C4RA01973C.

106. Zhao, M., et al., *Fabrication of Pd–Ni–P metallic glass nanoparticles and their application as highly durable catalysts in methanol electro-oxidation.* Chem. Mater., 2014. **26**(2): p. 1056-1061
107. Daimon, H. and Y. Kurobe, *Size reduction of PtRu catalyst particle deposited on carbon support by addition of non-metallic elements.* Catal. Today, 2006. **111**(3-4): p. 182-187 DOI: 10.1016/j.cattod.2005.10.023.
108. Yang, N., et al., *Amorphous/crystalline hetero‐phase Pd nanosheets: one‐pot synthesis and highly selective hydrogenation reaction.* Adv. Mater., 2018. **30**(39): p. 1803234
109. Zhao, X., et al., *Thiol treatment creates selective palladium catalysts for semihydrogenation of internal alkynes.* Chem, 2018. **4**(5): p. 1080-1091
110. Jin, M., et al., *Synthesis of Pd nanocrystals enclosed by {100} facets and with sizes< 10 nm for application in CO oxidation.* Nano Research, 2011. **4**(1): p. 83-91
111. Zhang, K., et al., *Fabrication of Pd/P nanoparticle networks with high activity for methanol oxidation.* Catalysis Science & Technology, 2016. **6**(16): p. 6441-6447
112. Zhao, Z., et al., *Synthesis of amorphous PdP nanoparticles supported on carbon nanospheres for 4-nitrophenol reduction in environmental applications.* Appl. Surf. Sci., 2018. **457**: p. 1009-1017
113. Zhao, M., Y. Ji, and N. Zhong, *Fabrication of ultrafine amorphous Pd-Ni-P nanoparticles supported on carbon nanotubes as an effective catalyst for electro-oxidation of methanol.* Int. J. Electrochem. Sci, 2016. **11**: p. 10488-10497
114. Rego, R., et al., *Development of PdP nano electrocatalysts for oxygen reduction reaction.* Electrochim. Acta, 2013. **87**: p. 73-81
115. Zhou, Y., et al., *Brand new P-doped gC 3 N 4: enhanced photocatalytic activity for H 2 evolution and Rhodamine B degradation under visible light.* Journal of Materials Chemistry A, 2015. **3**(7): p. 3862-3867
116. Zhang, J., Y. Xu, and B. Zhang, *Facile synthesis of 3D Pd–P nanoparticle networks with enhanced electrocatalytic performance towards formic acid electrooxidation.* Chem. Commun., 2014. **50**(88): p. 13451-13453 DOI: 10.1039/C4CC03282A.
117. Jiang, R., et al., *A class of (Pd–Ni–P) electrocatalysts for the ethanol oxidation reaction in alkaline media.* Acs Catalysis, 2014. **4**(8): p. 2577-2586
118. Yang, G., et al., *Preparation of carbon supported Pd–P catalyst with high content of element phosphorus and its electrocatalytic performance for formic acid oxidation.* Electrochem. Commun., 2010. **12**(3): p. 492-495
119. Huang, H., et al., *Exploring the role of nickel in the formation of amorphous Pt-based metallic alloys for methanol electro-oxidation with significant enhancement.* Electrochem. Commun., 2017. **82**: p. 107-111 DOI: https://doi.org/10.1016/j.elecom.2017.08.003.
120. Ma, Y., et al., *Ultrafine amorphous PtNiP nanoparticles supported on carbon as efficiency electrocatalyst for oxygen reduction reaction.* J. Power Sources, 2014. **259**: p. 87-91 DOI: https://doi.org/10.1016/j.jpowsour.2014.02.029.
121. Qi, Z. and W. Lee, *XPS study of CMP mechanisms of NiP coating for hard disk drive substrates.* Tribology international, 2010. **43**(4): p. 810-814
122. Ma, H., et al., *XPS and XANES characteristics of tribofilms and thermal films generated by two P-and/or S-containing additives in water-based lubricant.* Tribology international, 2009. **42**(6): p. 940-945
123. Huang, W., et al., *Highly active and durable methanol oxidation electrocatalyst based on the synergy of platinum–nickel hydroxide–graphene.* Nature communications, 2015. **6**(1): p. 1-8
124. Guo, L., et al., *A CO-tolerant PtRu catalyst supported on thiol-functionalized carbon nanotubes for the methanol oxidation reaction.* J. Power Sources, 2014. **247**: p. 360-364
125. Cao, L., et al., *Novel Nanocomposite Pt/RuO2· x H2O/Carbon Nanotube Catalysts for Direct Methanol Fuel Cells.* Angew. Chem. Int. Ed., 2006. **45**(32): p. 5315-5319

126. Maiyalagan, T., X. Wang, and A. Manthiram, *Highly active Pd and Pd–Au nanoparticles supported on functionalized graphene nanoplatelets for enhanced formic acid oxidation.* Rsc Advances, 2014. **4**(8): p. 4028-4033
127. Yang, J., et al., *An effective strategy for small-sized and highly-dispersed palladium nanoparticles supported on graphene with excellent performance for formic acid oxidation.* J. Mater. Chem., 2011. **21**(10): p. 3384-3390
128. Chakraborty, S. and C.R. Raj, *Electrocatalytic performance of carbon nanotube-supported palladium particles in the oxidation of formic acid and the reduction of oxygen.* Carbon, 2010. **48**(11): p. 3242-3249
129. Zhang, S., et al., *Electrostatic self‐assembly of a Pt‐around‐Au nanocomposite with high activity towards formic acid oxidation.* Angew. Chem. Int. Ed., 2010. **49**(12): p. 2211-2214
130. Mazumder, V. and S. Sun, *Oleylamine-mediated synthesis of Pd nanoparticles for catalytic formic acid oxidation.* J. Am. Chem. Soc., 2009. **131**(13): p. 4588-4589
131. Zhang, L., et al., *A carbon-supported Pd-P catalyst as the anodic catalyst in a direct formic acid fuel cell.* J. Power Sources, 2006. **162**(1): p. 177-179
132. Marković, N.M., et al., *Oxygen Reduction Reaction on Pt and Pt Bimetallic Surfaces: A Selective Review.* Fuel Cells, 2001. **1**(2): p. 105-116 DOI: 10.1002/1615-6854(200107)1:2<105::AID-FUCE105>3.0.CO;2-9.
133. Gasteiger, H.A., et al., *Activity benchmarks and requirements for Pt, Pt-alloy, and non-Pt oxygen reduction catalysts for PEMFCs.* Applied Catalysis B: Environmental, 2005. **56**(1-2): p. 9-35
134. Nørskov, J.K., et al., *Origin of the Overpotential for Oxygen Reduction at a Fuel-Cell Cathode.* The Journal of Physical Chemistry B, 2004. **108**(46): p. 17886-17892 DOI: 10.1021/jp047349j.
135. Greeley, J., et al., *Alloys of platinum and early transition metals as oxygen reduction electrocatalysts.* Nature Chemistry, 2009. **1**(7): p. 552-556 DOI: 10.1038/nchem.367.
136. Stamenkovic, V.R., et al., *Trends in electrocatalysis on extended and nanoscale Pt-bimetallic alloy surfaces.* Nature Materials, 2007. **6**(3): p. 241-247 DOI: 10.1038/nmat1840.
137. Tian, N., et al., *Synthesis of tetrahexahedral platinum nanocrystals with high-index facets and high electro-oxidation activity.* Science, 2007. **316**(5825): p. 732-5 DOI: 10.1126/science.1140484.
138. Somorjai, G.A. and D.W. Blakely, *Mechanism of catalysis of hydrocarbon reactions by platinum surfaces.* Nature, 1975. **258**(5536): p. 580-583 DOI: 10.1038/258580a0.
139. Quan, Z., Y. Wang, and J. Fang, *High-Index Faceted Noble Metal Nanocrystals.* Acc. Chem. Res., 2013. **46**(2): p. 191-202 DOI: 10.1021/ar200293n.
140. Gao, G., S. Bottle, and A. Du, *Understanding the activity and selectivity of single atom catalysts for hydrogen and oxygen evolution via ab initial study.* Catalysis Science & Technology, 2018. **8**(4): p. 996-1001 DOI: 10.1039/C7CY02463K.
141. Falicov, L. and G. Somorjai, *Correlation between catalytic activity and bonding and coordination number of atoms and molecules on transition metal surfaces: Theory and experimental evidence.* Proceedings of the National Academy of Sciences, 1985. **82**(8): p. 2207-2211
142. Kuzume, A., E. Herrero, and J.M. Feliu, *Oxygen reduction on stepped platinum surfaces in acidic media.* Journal of Electroanalytical Chemistry, 2007. **599**(2): p. 333-343 DOI: https://doi.org/10.1016/j.jelechem.2006.05.006.
143. Kesmodel, L.L. and L.M. Falicov, *The electronic potential in a metal close to a surface edge.* Solid State Communications, 1975. **16**(10): p. 1201-1204 DOI: https://doi.org/10.1016/0038-1098(75)90146-5.
144. Painter, G.S., P.J. Jennings, and R.O. Jones, *Electronic structure of stepped transition metal surfaces.* Journal of Physics C: Solid State Physics, 1975. **8**(10): p. L199-L202 DOI: 10.1088/0022-3719/8/10/019.

145. Sun, S.-G., et al., *Electrocatalytic properties of Pt (111), Pt (332), Pt (331) and Pt (110) single crystal electrodes towards ethylene glycol oxidation in sulphuric acid solutions.* Journal of Electroanalytical Chemistry, 1992. **340**(1-2): p. 213-226
146. Richter, B., et al., *Cluster core-level binding-energy shifts: the role of lattice strain.* Phys. Rev. Lett., 2004. **93**(2): p. 026805
147. Jeong, H.J., et al., *Platinum–ruthenium heterogeneous catalytic anodes prepared by atomic layer deposition for use in direct methanol solid oxide fuel cells.* ACS Catalysis, 2015. **5**(3): p. 1914-1921
148. Hsin, Y.L., K.C. Hwang, and C.-T. Yeh, *Poly (vinylpyrrolidone)-modified graphite carbon nanofibers as promising supports for PtRu catalysts in direct methanol fuel cells.* J. Am. Chem. Soc., 2007. **129**(32): p. 9999-10010
149. Dameron, A.A., et al., *Pt–Ru alloyed fuel cell catalysts sputtered from a single alloyed target.* Acs Catalysis, 2011. **1**(10): p. 1307-1315
150. Zheng, J., et al., *Platinum–ruthenium nanotubes and platinum–ruthenium coated copper nanowires as efficient catalysts for electro-oxidation of methanol.* Acs Catalysis, 2015. **5**(3): p. 1468-1474
151. Melvin, A.A., et al., *Electrocatalyst on insulating support?: hollow silica spheres loaded with Pt nanoparticles for methanol oxidation.* ACS Applied Materials & Interfaces, 2015. **7**(12): p. 6590-6595
152. Zhao, Y., et al., *Revisiting the oxidation peak in the cathodic scan of the cyclic voltammogram of alcohol oxidation on noble metal electrodes.* RSC advances, 2016. **6**(7): p. 5384-5390
153. Xu, C., et al., *Nanotubular Mesoporous PdCu Bimetallic Electrocatalysts toward Oxygen Reduction Reaction.* Chem. Mater., 2009. **21**(14): p. 3110-3116 DOI: 10.1021/cm900244g.
154. Tan, Y., et al., *Monolayer MoS2 Films Supported by 3D Nanoporous Metals for High-Efficiency Electrocatalytic Hydrogen Production.* Adv. Mater., 2014. **26**(47): p. 8023-8028 DOI: 10.1002/adma.201403808.
155. Hu, Y.C., et al., *A highly efficient and self‐stabilizing metallic‐glass catalyst for electrochemical hydrogen generation.* Adv. Mater., 2016. **28**(46): p. 10293-10297
156. Wang, A.-L., et al., *Design of Pd/PANI/Pd sandwich-structured nanotube array catalysts with special shape effects and synergistic effects for ethanol electrooxidation.* J. Am. Chem. Soc., 2013. **135**(29): p. 10703-10709
157. Yin, M., et al., *Tungsten carbide promoted Pd and Pd–Co electrocatalysts for formic acid electrooxidation.* J. Power Sources, 2012. **219**: p. 106-111
158. Bianchini, C. and P.K. Shen, *Palladium-based electrocatalysts for alcohol oxidation in half cells and in direct alcohol fuel cells.* Chem. Rev., 2009. **109**(9): p. 4183-4206
159. Zhou, W.P., et al., *Size effects in electronic and catalytic properties of unsupported palladium nanoparticles in electrooxidation of formic acid.* The Journal of Physical Chemistry B, 2006. **110**(27): p. 13393-13398
160. Zhao, Y., et al., *Amorphous CuPt Alloy Nanotubes Induced by Na2S2O3 as Efficient Catalysts for Methanol Oxidation Reaction.* ACS Catalysis, 2016. **6** DOI: 10.1021/acscatal.6b00540.
161. Antolini, E., *Palladium in fuel cell catalysis.* Energy & Environmental Science, 2009. **2**(9): p. 915-931
162. Chang, J., et al., *An effective Pd–Ni2P/C anode catalyst for direct formic acid fuel cells.* Angew. Chem. Int. Ed., 2014. **53**(1): p. 122-126
163. Huang, Z., et al., *Au-supported Pt–Au mixed atomic monolayer electrocatalyst with ultrahigh specific activity for oxidation of formic acid in acidic solution.* Chem. Commun., 2012. **48**(99): p. 12106-12108
164. Matin, M.A., J.-H. Jang, and Y.-U. Kwon, *PdM nanoparticles (M= Ni, Co, Fe, Mn) with high activity and stability in formic acid oxidation synthesized by sonochemical reactions.* J. Power Sources, 2014. **262**: p. 356-363

165. Zhang, L.Y., et al., *Perforated Pd Nanosheets with Crystalline/Amorphous Heterostructures as a Highly Active Robust Catalyst toward Formic Acid Oxidation.* Small, 2019. **15**(47): p. 1904245 DOI: 10.1002/smll.201904245.
166. Guo, S., et al., *Co/CoO nanoparticles assembled on graphene for electrochemical reduction of oxygen.* Angew. Chem., 2012. **124**(47): p. 11940-11943
167. Vo Doan, T.T., et al., *Theoretical Modelling and Facile Synthesis of a Highly Active Boron-Doped Palladium Catalyst for the Oxygen Reduction Reaction.* Angew. Chem. Int. Ed., 2016. **55**(24): p. 6842-6847 DOI: 10.1002/anie.201601727.
168. Jasinski, R., *A New Fuel Cell Cathode Catalyst.* Nature, 1964. **201**(4925): p. 1212-1213 DOI: 10.1038/2011212a0.
169. Dombrovskis, J.K., et al., *Transition Metal Ion-Chelating Ordered Mesoporous Carbons as Noble Metal-Free Fuel Cell Catalysts.* Chem. Mater., 2013. **25**(6): p. 856-861 DOI: 10.1021/cm303357p.